Biochemical and Biophysical Research Communications xxx (2013) xxx–xxx

Contents lists available at ScienceDirect

Biochemical and Biophysical Research Communications

journal homepage: www.elsevier.com/locate/ybbrc

Uric acid induces NADPH oxidase-independent neutrophil extracellular trap formation

Yasuyuki Arai [a,1], Yoko Nishinaka [b,c,1], Toshiyuki Arai [a,d], Makiko Morita [b], Kiyomi Mizugishi [a], Souichi Adachi [b], Akifumi Takaori-Kondo [a], Tomohiro Watanabe [e], Kouhei Yamashita [a,*]

[a] Department of Hematology and Oncology, Graduate School of Medicine, Kyoto University, Kyoto 606-8507, Japan
[b] Human Health Science, Graduate School of Medicine, Kyoto University, Kyoto 606-8507, Japan
[c] Department of Clinical Application, Center for iPS Cell Research and Application, Kyoto University, Kyoto 606-8507, Japan
[d] Department of Anesthesia, Kyoto City Hospital, Kyoto 604-8845, Japan
[e] Center for Innovation in Immunoregulative Technology and Therapeutics, Graduate School of Medicine, Kyoto University, Kyoto 606-8507, Japan

ARTICLE INFO

Article history:
Received 15 November 2013
Available online xxxx

Keywords:
Uric acid
Neutrophil extracellular trap formation
NADPH oxidase
Chronic granulomatous disease
NF-κB
Reactive oxygen species

ABSTRACT

Neutrophil extracellular traps (NETs) are composed of extracellular DNA fibers with antimicrobial peptides that capture and kill microbes. NETs play a critical role in innate host defense and in autoimmune and inflammatory diseases. While the mechanism of NET formation remains unclear, reactive oxygen species (ROS) produced via activation of NADPH oxidase (Nox) are known to be an important requirement. In this study, we investigated the effect of uric acid (UA) on NET formation. UA, a well-known ROS scavenger, was found to suppress Nox-dependent ROS release in a dose-dependent manner. Low concentrations of UA significantly inhibited Nox-dependent NET formation. However, high concentrations of UA unexpectedly induced, rather than inhibited, NET formation. NETs were directly induced by UA alone in a Nox-independent manner, as revealed by experiments using control neutrophils treated with ROS inhibitors or neutrophils of patients with chronic granulomatous disease who have a congenital defect in ROS production. Furthermore, we found that UA-induced NET formation was partially mediated by NF-κB activation. Our study is the first to demonstrate the novel function of UA in NET formation and may provide insight into the management of patients with hyperuricemia.

1. Introduction

Neutrophils, the first line of defense against the microbes, play a critical role in innate immunity [1]. In infected sites, they phagocytose microbes, degranulate enzymes, and produce reactive oxygen species (ROS) such as superoxide and hydrogen peroxide generated by the NADPH oxidase (Nox) complex. Recently, a novel killing mechanism known as neutrophil extracellular traps (NETs) has been reported. NETs capture microbes with their extracellular structures consisting of DNA fibers and antimicrobial granule proteins [2,3]. Many physiological stimuli are known to induce NETs. Notably, NET formation is generally ROS-dependent. Patients with chronic granulomatous disease (CGD), who are defective in Nox activity, fail to generate ROS and to make NETs [4]. In a recent study, we demonstrated that singlet oxygen ($^1O_2$), one species of ROS, is required for Nox-dependent NET formation on stimulation with phorbol myristate acetate (PMA) [5]. Interestingly, neutrophils of CGD patients treated with $^1O_2$ *in vitro* produced NETs, revealing that the pathway could be rescued downstream of Nox [5].

Uric acid (UA), a product of purine metabolism, is a scavenger of $^1O_2$ that regulates oxidative stress in humans [6]. Since $^1O_2$ is produced by Nox [7], UA is expected to suppress Nox-dependent NET formation. However, a recent study showed that peripheral and synovial fluid neutrophils derived from patients with acute gout, whose UA levels in serum were mostly high, formed NETs [8]. Acute gout is an inflammatory arthritis that is triggered by the deposition of monosodium urate (MSU) crystals, uric acid precipitates in sodium, into the joint space. The inflammatory cascade results in the secretion of inflammatory cytokines, especially interleukin (IL)-1ß and neutrophil recruitment into the joint [9]. Thus, it is still a matter of debate what effect UA directly exerts on NET formation.

In the present study, we first examined the effect of UA on Nox-dependent NET formation by control neutrophils stimulated with PMA. Thereafter, we investigated how UA directly affected NET for-

Abbreviations: CGD, chronic granulomatous disease; DHR, dihydrorhodamine 123; DPI, diphenyleneiodonium; HBSS, Hanks' balanced salt solution; MSU, monosodium urate; MVP, trans-1-(2′-methoxyvinyl)pyrene; Nox, NADPH oxidase; NET, neutrophil extracellular trap; PBN, α-phenyl-*N*-tert-butyl nitrone; PMA, phorbol myristate acetate; ROS, reactive oxygen species; $^1O_2$, singlet oxygen; UA, uric acid.

* Corresponding author. Fax: +81 75 751 4963.
E-mail address: kouhei@kuhp.kyoto-u.ac.jp (K. Yamashita).

[1] These authors contributed equally to this work.

0006-291X/$ - see front matter © 2013 Elsevier Inc. All rights reserved.
http://dx.doi.org/10.1016/j.bbrc.2013.12.007

mation by using control neutrophils treated with ROS inhibitors or CGD neutrophils. Finally, we demonstrate that UA may induce NET formation in a manner distinct from that of PMA.

2. Materials and methods

2.1. Reagents

Hanks' balanced salt solution (HBSS) was purchased from Invitrogen (Carlsbad, CA, USA); trans-1-(2′-methoxyvinyl)pyrene (MVP), Sytox green and orange (for double-strand DNA staining), and dihydrorhodamine 123 (DHR) were ordered from Molecular Probes (Eugene, OR, USA). α-Phenyl-*N*-tert-butyl nitrone (PBN) was acquired from Radical Research Ltd. (Hino, Tokyo, Japan) and was dissolved in phosphate-buffered saline (PBS) at a final concentration of 100 mM (pH 7.4). Anti-myeloperoxidase (MPO) antibody and matched secondary antibody (anti-rabbit IgG-Alexa Fluor 488) were obtained from Abcam (Eugene, OR, USA) and Life Technologies (Carlsbad, CA, USA), respectively. Other chemicals, including UA, PMA, diphenyleneiodonium (DPI), and apocynin, were purchased from Sigma Aldrich Inc. (St. Louis, MO, USA). (*E*)3-[(4-Methylphenyl)sulfonyl]-2-propenenitrile (BAY 11-7082) was obtained from Merck (Darmstadt, Germany).

2.2. Human CGD patients

We studied two CGD patients, a 29-year-old man with gp91-phox deficiency with a G-to-A point mutation at nucleotide 252 in exon 3, and a 24-year-old man with gp91-phox deficiency with a G-to-A point mutation at nucleotide 389 in exon 10.

2.3. Isolation of human neutrophils

Human neutrophils were isolated from peripheral blood by sedimentation through two-step Percoll (GE Healthcare, Tokyo, Japan) gradients. The experiments were conducted with the understanding and the consent of each participant. The ethical committee of Kyoto University approved the experiments.

2.4. Chemiluminescence assay

Neutrophils (2×10^6 cells) were mounted on a luminescence reader (Aloka BLR-310; Aloka, Tokyo, Japan) in the presence of 40 μM MVP, a $^1O_2$-specific probe [10]. After that, neutrophils were stimulated with 100 ng/ml PMA in the presence of 0–5 mg/dl UA, or 8 mg/dl UA alone, and MVP luminescence was monitored every 30 s for 30 min.

2.5. Flow cytometric DHR assay

Neutrophils (1×10^6 cells) treated with 2 μM DHR were stimulated with 100 ng/ml PMA or 8 mg/dl UA for 30 min at 37 °C and analyzed by flow cytometry using a FACSCanto II (Becton Dickinson, Durham, NC, USA).

2.6. Immunofluorescence stainings of NET-forming neutrophils

Purified neutrophils (1×10^5 cells) were incubated with 100 ng/ml PMA or 8 mg/dl UA in HBSS without serum for 3 h on culture slides (BD Biosciences, San Jose, CA, USA). After fixation with 2% paraformaldehyde (Nacalai Tesque, Kyoto, Japan) for 15 min and

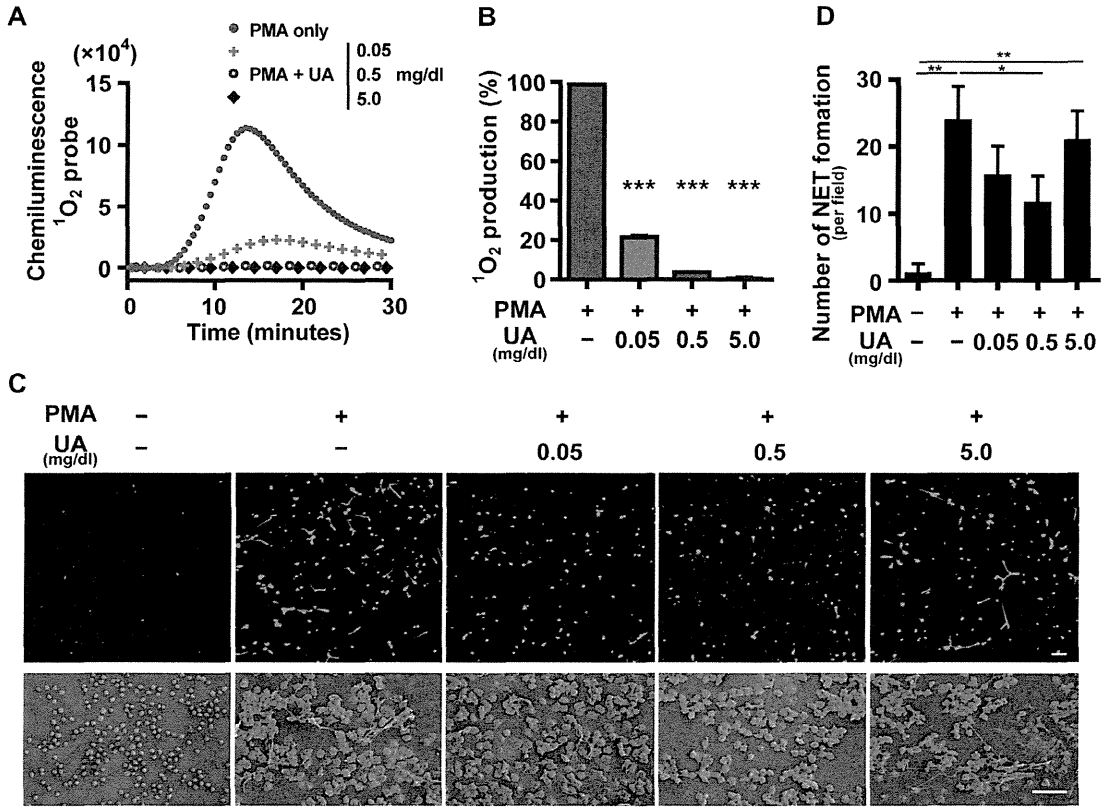

Fig. 1. The effect of UA on PMA-induced ROS production and NET formation. Neutrophils were isolated from the peripheral blood of healthy volunteers. (A) The effect of UA (0–5 mg/dl) on $^1O_2$ production by PMA-stimulated neutrophils. The $^1O_2$ production by neutrophils was examined by chemiluminescence using a $^1O_2$-specific probe, MVP. (B) Quantitative analysis of $^1O_2$ production by neutrophils. The $^1O_2$ production is shown relative to that by PMA-stimulated neutrophils in the absence of UA. The data represent the mean ± SE ($n = 3$, $^{***}P < 0.001$, unpaired *t*-test). (C) The effect of UA on PMA-induced NET formation. Neutrophils stimulated with PMA were incubated with 0–5 mg/dl UA. NET formation was visualized by laser-scanning fluorescence confocal microscopy (upper panels) and SEM (lower panels). Scale bars represent 100 μm (upper panels) and 30 μm (lower panels). (D) Quantitative analysis of NET formation. The data represent the mean ± SE ($n = 4$, $^{*}P < 0.05$, $^{**}P < 0.01$, unpaired *t*-test).

Please cite this article in press as: Y. Arai et al., Uric acid induces NADPH oxidase-independent neutrophil extracellular trap formation, Biochem. Biophys. Res. Commun. (2013), http://dx.doi.org/10.1016/j.bbrc.2013.12.007

permeabilization with 100% methanol (Nacalai Tesque) for 10 min at -20 °C, the cells were stained with rabbit anti-MPO antibodies overnight at 4 °C, followed by Alexa Fluor 488-conjugated goat anti-rabbit IgG and Sytox orange. The cells were attached to the slides by centrifugation, coverslipped with mounting medium (ProLong Gold Antifade Reagent, Life Technologies), and analyzed by confocal microscopy.

2.7. NET formation by neutrophils

Neutrophils (4×10^6 cells) from healthy volunteers were suspended in HBSS without serum and stimulated with 100 ng/ml PMA in the presence of 0–5 mg/dl UA for 3 h at 37 °C under 5% CO_2 in glass base dish (Asahi Glass, Tokyo, Japan). In other experiments, neutrophils from healthy volunteers or CGD patients were stimulated with 1–8 mg/dl UA alone. After incubation, cells were stained with 500 nM Sytox Green, and NET formation was visualized with a laser-scanning fluorescence confocal microscope (Nikon Digital Eclipse C1, Tokyo, Japan). Quantitative analysis was performed by counting the number of NET-forming cells per field (average data of 5 randomly selected fields). NET formation was also visualized with a scanning electron microscope (SEM, S-4700, Hitachi, Tokyo, Japan).

2.8. Treatments of neutrophils with inhibitors

Neutrophils (4×10^6 cells) from healthy volunteers were pre-incubated at 37 °C for 30 min with Nox inhibitors, DPI (10 μM) and apocynin (10 μM), a $^1O_2$ inhibitor, PBN (4 mM) [11], or an NF-κB inhibitor, Bay 11-7082 (10 μM), and then stimulated with 100 ng/ml PMA or 8 mg/dl UA for 3 h. NET formation was visualized and analyzed as described above.

2.9. Immunoblotting

Neutrophils (4×10^6 cells) from healthy volunteers were incubated at 37 °C for 30 min with 100 ng/ml PMA or 8 mg/dl UA. Lysates were prepared using RIPA lysis buffer (Wako Pure Chemical Industries, Osaka, Japan). Cell debris was separated by centrifugation and equal amounts of proteins in the supernatant were separated by electrophoresis (4–12% SDS–polyacrylamide gels, Life Technologies). Proteins were then electrotransferred onto nitrocel-

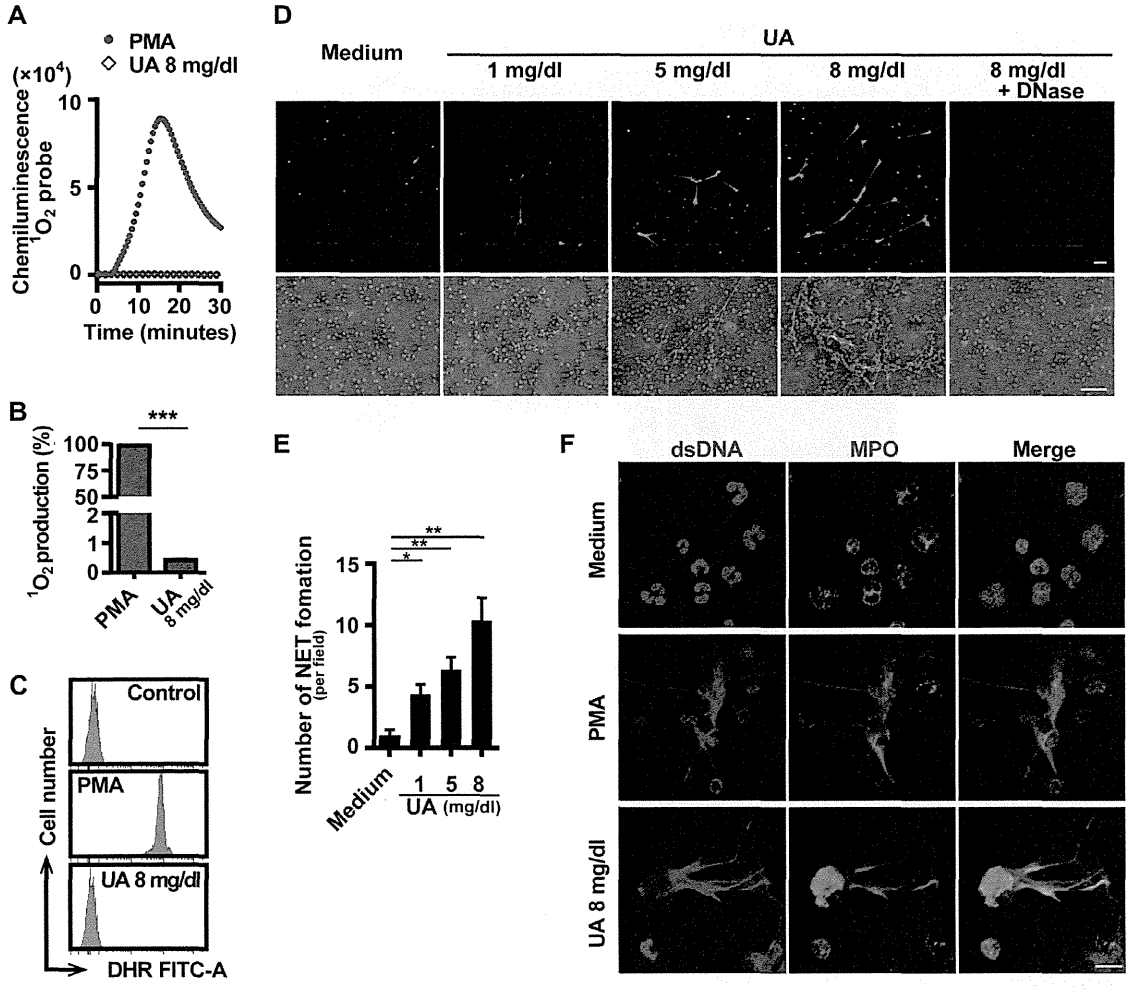

Fig. 2. The effect of UA alone on ROS production and NET formation. (A and B) Effect of UA on $^1O_2$ production. Neutrophils were stimulated with PMA (100 ng/ml) or UA (8 mg/dl). $^1O_2$ production was examined by chemiluminescence using a $^1O_2$-specific probe, MVP. (A) Representative data. UA-stimulated neutrophils hardly produced any $^1O_2$. (B) Quantitative analysis of $^1O_2$ production shown relative to that by PMA-stimulated neutrophils. Data represent mean ± SE ($n = 3$, $^{***}P < 0.001$, unpaired t-test). (C) ROS production by DHR assay. The logarithmic fluorescence intensity is shown on the x-axis and the cell count on the y-axis. (D–F) Direct effect of UA on NET formation. (D) Representative micrographs of neutrophils incubated with 1–8 mg/dl of UA. NET formation was visualized by laser-scanning fluorescence confocal microscopy (upper panels) and SEM (lower panels). Scale bars represent 100 μm (upper panels) and 30 μm (lower panels). (E) Quantitative analysis of NET formation. Data represent the mean ± SE ($n = 5$, $^{*}P < 0.05$, $^{**}P < 0.01$, unpaired t-test). (F) Colocalization of extracellular dsDNA and MPO in UA-stimulated neutrophils. UA- or PMA-stimulated neutrophils were immunostained with anti-MPO antibody (green). The dsDNAs were counterstained with Sytox-orange (red). Scale bars represent 10 μm. (For interpretation of the references to color in this figure legend, the reader is referred to the web version of this article.)

Please cite this article in press as: Y. Arai et al., Uric acid induces NADPH oxidase-independent neutrophil extracellular trap formation, Biochem. Biophys. Res. Commun. (2013), http://dx.doi.org/10.1016/j.bbrc.2013.12.007

lulose membranes. After blocking, membranes were incubated overnight at 4 °C with a rabbit polyclonal anti-phospho-NF-κB p65 or anti-NF-κB p65 antibody (Santa Cruz Biotechnology, Dallas, TX, USA) followed by a goat anti-rabbit HRP antibody. Protein bands were visualized by enhanced chemiluminescence, and results were analyzed with ImageJ software.

2.10. Statistical analysis

Data were expressed as mean ± standard error (SE). Values of $P < 0.05$ determined by the unpaired Student t-test were considered significant.

3. Results and discussion

We examined the effect of UA on $^1O_2$ production and NET formation by PMA-stimulated neutrophils. First, neutrophils from healthy volunteers were stimulated with PMA with or without UA, and the $^1O_2$ production was detected by chemiluminescence. As expected, increasing concentrations of UA (0.05–5 mg/dl) suppressed $^1O_2$ production by PMA-stimulated neutrophils in a dose-dependent manner, suggesting that UA is a $^1O_2$ scavenger (Fig. 1A and B). Treatments of less than 0.5 mg/dl of UA suppressed PMA-induced NET formation in confocal microscopy (Fig. 1C, upper panels, and Fig. 1D) and SEM (Fig. 1C, lower panels). Surprisingly, treatment of PMA-stimulated neutrophils with 5 mg/dl of UA failed to suppress NET formation, suggesting that a high concentration of UA may have a novel function in NET formation (Fig. 1C and D). These results were substantiated by the quantitative analysis of representative micrographs (Fig. 1D).

Next, we investigated the direct effect of UA on $^1O_2$ production and NET formation. UA treatment alone did not produce any detectable levels of $^1O_2$ (Fig. 2A and B). We used the fluorescent dye DHR in a flow cytometric assay to detect ROS. UA-stimulated neutrophils from healthy volunteers did not exhibit any increase in DHR fluorescence, in contrast to a significant increase in PMA-stimulated neutrophils (Fig. 2C). Unexpectedly, UA alone

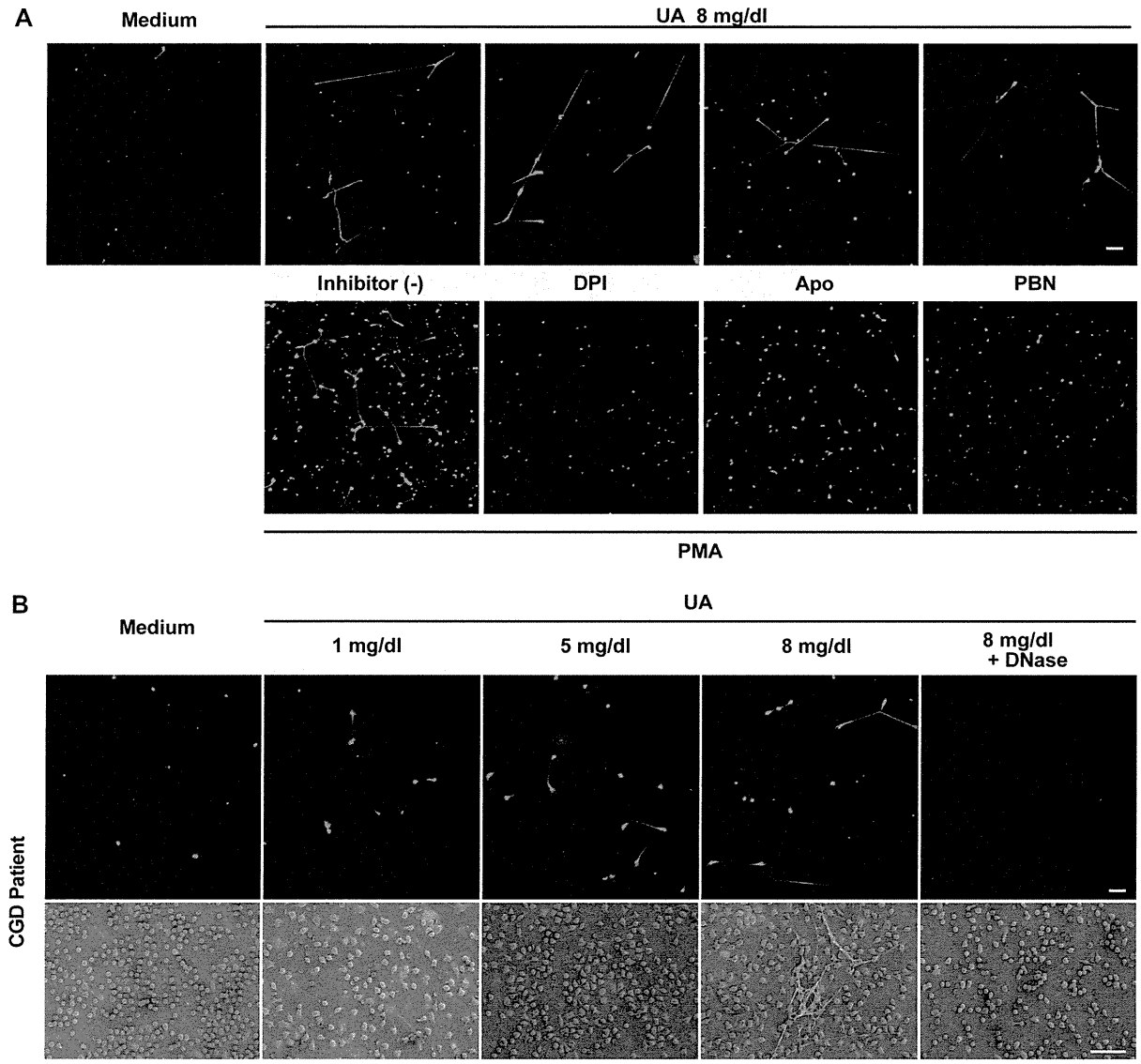

Fig. 3. UA-induced NET formation is independent of ROS. (A) The effect of ROS inhibitors on UA- (upper panels) or PMA- (lower panels) induced NET formation. Neutrophils from healthy volunteers were incubated with 8 mg/dl UA or 100 ng/ml PMA in the presence or absence of Nox inhibitors, DPI and apocynin (Apo), or a $^1O_2$ inhibitor, PBN. NET formation was visualized by laser-scanning fluorescence confocal microscopy. Scale bars represent 100 μm. (B) The effect of UA on NET formation. Neutrophils from CGD patients were incubated with 1–8 mg/dl of UA. Representative micrographs are shown. NET formation was visualized by laser-scanning fluorescence confocal microscopy (upper panels) and SEM (lower panels). Scale bars represent 100 μm (upper panels) and 30 μm (lower panels).

Please cite this article in press as: Y. Arai et al., Uric acid induces NADPH oxidase-independent neutrophil extracellular trap formation, Biochem. Biophys. Res. Commun. (2013), http://dx.doi.org/10.1016/j.bbrc.2013.12.007

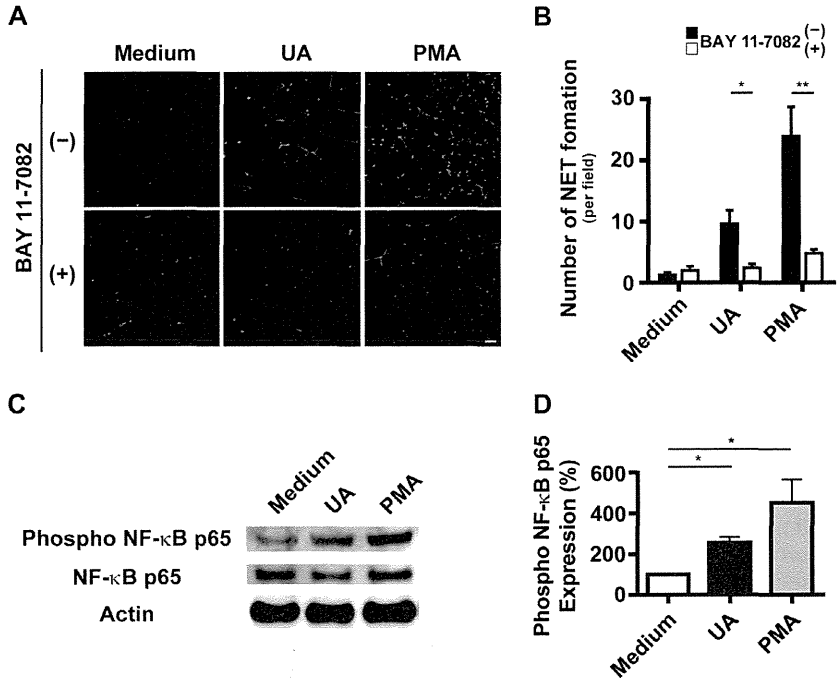

Fig. 4. UA induces NET formation through NF-κB activation. (A and B) The effect of an NF-κB inhibitor on UA-induced NET formation. Neutrophils from healthy volunteers were stimulated with 100 ng/ml PMA or 8 mg/dl UA in the presence or absence of an NF-κB inhibitor. (A) Representative micrographs. NET formation was visualized by laser-scanning fluorescence confocal microscopy. Scale bars represent 100 μm. (B) Quantitative analysis of NET formation. The data represent the mean ± SE ($n = 5$, $^*P < 0.05$, $^{**}P < 0.01$, unpaired t-test). (C) Immunoblot analysis of PMA- or UA-stimulated neutrophils. Cell lysates were subjected to immunoblotting using an anti-phospho-NF-κB p65 or anti-NF-κB p65 antibody. Membranes were reprobed with an anti-actin antibody. (D) Quantification of proteins on immunoblots. The expression levels are shown relative to that in neutrophils without stimuli. The data represent the mean ± SE ($n = 5$, $^*P < 0.05$, unpaired t-test).

significantly induced NET formation in healthy neutrophils, irrespective of the absence of ROS (Fig. 2D and E). NET formation was abrogated by DNase treatment, which degrades DNA fibers of NETs (Fig. 2D). NET formation by UA was further verified by immunostaining, in which extracellular dsDNA colocalized with a granule protein MPO, an important structural component of NETs (Fig. 2F). These results suggest that NET formation by UA may not be mediated by ROS.

This hypothesis was substantiated by the use of Nox inhibitors, DPI and apocynin, or a $^1O_2$ scavenger, PBN. None of the ROS inhibitors suppressed UA-induced NET formation, while PMA-induced NETs were strongly inhibited (Fig. 3A). We next examined NET formation in neutrophils from CGD patients, who have a defect in ROS formation. Regardless of the absence of ROS, CGD neutrophils treated with UA produced NETs, which were suppressed by DNase treatment (Fig. 3B). Taken together, these results suggest that UA may induce NET formation in a Nox-independent manner.

Recently, Lopponi et al. implicated NF-κB activation in NET formation induced by PMA stimulus or stress signals, such as acidic or hyperthermic conditions [12]. Therefore, we investigated whether NF-κB blockade affected NET formation by UA-stimulated neutrophils. The treatment of healthy neutrophils with the NF-κB inhibitor BAY 11-7082 resulted in a marked suppression of UA-induced NET formation (Fig. 4A and B). In addition, immunoblot analysis revealed that phosphorylation of the p65 subunit of NF-κB was significantly enhanced in neutrophils stimulated with UA (Fig. 4C and D). Taken together, these results suggest that the NF-κB cascade is important in UA-mediated NET formation, and could be a key regulatory pathway of NET formation. Identification of signaling pathways upstream of NF-κB in UA-induced NET formation should be a future area of investigation.

In summary, this is the first report to demonstrate the novel function of UA in NET formation. Contrary to expectations, UA, a known $^1O_2$ scavenger, induced NETs in neutrophils in a Nox-independent manner and partially through activation of the NF-κB pathway. The mechanisms by which UA contributes to NET formation are not yet clear. It has been reported that the Raf-MEK-ERK pathway is involved in a NET formation cascade downstream of Nox activation in PMA-stimulated neutrophils [13]. Furthermore, MSU crystals induced NETs in a ROS-dependent manner as well as PMA [14]. In contrast, NET formation by UA was independent of ROS. In addition, neither the activation of ERK, nor the suppression of NETs by an ERK inhibitor, was observed in UA-stimulated neutrophils in our study (unpublished observation). This suggests that UA induces NETs in a different fashion from that of PMA and MSU crystals. An example of ROS-independent NET formation was reported in a recent study, where the calcium ionophore ionomycin did not require Nox activation to induce NETs [15]. Moreover, *Staphylococcus aureus* and *Candida albicans* have been reported to induce NETs independently of Nox [16,17]. Thus, it is possible that there are several mechanisms of NET formation. The importance of a ROS-independent pathway in NET formation in physiological settings awaits further investigation.

NETs are similar to a double-edged sword; they can either fight disease or cause disease, depending on the situation [18]. Excessive NET formation is associated with the pathogenesis of inflammatory and autoimmune diseases, including preeclampsia [19], cystic fibrosis [20], and systemic lupus erythematosus [21]. Moreover, NETs are relevant to vascular injury, in which extracellular histones released from neutrophils during NET formation injure the endothelium [22], and the injured endothelium, in turn, induces NETs, establishing a vicious cycle leading to severe damage [23]. Clinically, the association of hyperuricemia and gout with other medical conditions such as hypertension, chronic kidney disease, and cardiovascular disease has been recognized [24]. Recent animal and epidemiologic studies support the idea that uric acid elevation in the serum is an independent risk factor for the development of these serious medical problems, by damaging

Please cite this article in press as: Y. Arai et al., Uric acid induces NADPH oxidase-independent neutrophil extracellular trap formation, Biochem. Biophys. Res. Commun. (2013), http://dx.doi.org/10.1016/j.bbrc.2013.12.007

endothelial cells, although it is still a matter of debate [25]. In light of these findings, we speculate that uric acid elevation may induce NET formation and subsequent vascular endothelial dysfunction, ultimately leading to cardiovascular diseases. Therefore, NETs could be a missing link between uric acid elevation and cardiovascular diseases. Thus, we may need to reappraise the importance of uric acid in human health and disease, and reconsider the management of patients with asymptomatic hyperuricemia in order to decrease the risk of cardiovascular diseases.

Conflict of interest disclosure

The authors declare no conflict of interest.

Acknowledgments

We thank Keiko Furuta and Haruyasu Kohda (Division of Electron Microscopic Study, Center for Anatomical Studies, Graduate School of Medicine, Kyoto University) for excellent technical assistance. This research was supported by Grants-in-aid for scientific research from the Japan Society for the Promotion of Science (23591474) to K.Y.

References

[1] C. Nathan, Neutrophils and immunity: challenges and opportunities, Nat. Rev. Immunol. 6 (2006) 173–182.
[2] V. Brinkmann, U. Reichard, C. Goosmann, B. Fauler, Y. Uhlemann, D.S. Weiss, Y. Weinrauch, A. Zychlinsky, Neutrophil extracellular traps kill bacteria, Science 303 (2004) 1532–1535.
[3] V. Brinkmann, A. Zychlinsky, Beneficial suicide: why neutrophils die to make NETs, Nat. Rev. Microbiol. 5 (2007) 577–582.
[4] T.A. Fuchs, U. Abed, C. Goosmann, R. Hurwitz, I. Schulze, V. Wahn, Y. Weinrauch, V. Brinkmann, A. Zychlinsky, Novel cell death program leads to neutrophil extracellular traps, J. Cell Biol. 176 (2007) 231–241.
[5] Y. Nishinaka, T. Arai, S. Adachi, A. Takaori-Kondo, K. Yamashita, Singlet oxygen is essential for neutrophil extracellular trap formation, Biochem. Biophys. Res. Commun. 413 (2011) 75–79.
[6] B.N. Ames, R. Cathcart, E. Schwiers, P. Hochstein, Uric acid provides an antioxidant defense in humans against oxidant- and radical-caused aging and cancer: a hypothesis, Proc. Natl. Acad. Sci. U.S.A. 78 (1981) 6858–6862.
[7] S.J. Klebanoff, Myeloperoxidase: friend and foe, J. Leukocyte Biol. 77 (2005) 598–625.
[8] I. Mitroulis, K. Kambas, A. Chrysanthopoulou, P. Skendros, E. Apostolidou, I. Kourtzelis, G.I. Drosos, D.T. Boumpas, K. Ritis, Neutrophil extracellular trap formation is associated with IL-1beta and autophagy-related signaling in gout, PLoS One 6 (2011) e29318.
[9] E.B. Gonzalez, An update on the pathology and clinical management of gouty arthritis, Clin. Rheumatol. 31 (2012) 13–21.
[10] G.H. Posner, J.R. Lever, K. Miura, C. Lisek, H.H. Seliger, A. Thompson, A chemiluminescent probe specific for singlet oxygen, Biochem. Biophys. Res. Commun. 123 (1984) 869–873.
[11] A. Kawai, Y. Nishinaka, T. Arai, K. Hirota, H. Mori, N. Endo, T. Miyoshi, K. Yamashita, M. Sasada, Alpha-phenyl-*N*-tert-butyl nitrone has scavenging activity against singlet oxygen ((1)O(2)) and attenuates (1)O(2)-induced neuronal cell death, J. Pharmacol. Sci. 108 (2008) 545–549.
[12] M.J. Lapponi, A. Carestia, V.I. Landoni, L. Rivadeneyra, J. Etulain, S. Negrotto, R.G. Pozner, M. Schattner, Regulation of neutrophil extracellular trap formation by anti-inflammatory drugs, J. Pharmacol. Exp. Ther. 345 (2013) 430–437.
[13] A. Hakkim, T.A. Fuchs, N.E. Martinez, S. Hess, H. Prinz, A. Zychlinsky, H. Waldmann, Activation of the Raf-MEK-ERK pathway is required for neutrophil extracellular trap formation, Nat. Chem. Biol. 7 (2011) 75–77.
[14] C. Schorn, C. Janko, V. Krenn, Y. Zhao, L.E. Munoz, G. Schett, M. Herrmann, Bonding the foe – NETting neutrophils immobilize the pro-inflammatory monosodium urate crystals, Front. Immunol. 3 (2012) 376.
[15] H. Parker, M. Dragunow, M.B. Hampton, A.J. Kettle, C.C. Winterbourn, Requirements for NADPH oxidase and myeloperoxidase in neutrophil extracellular trap formation differ depending on the stimulus, J. Leukocyte Biol. 92 (2012) 841–849.
[16] F.H. Pilsczek, D. Salina, K.K. Poon, C. Fahey, B.G. Yipp, C.D. Sibley, S.M. Robbins, F.H. Green, M.G. Surette, M. Sugai, M.G. Bowden, M. Hussain, K. Zhang, P. Kubes, A novel mechanism of rapid nuclear neutrophil extracellular trap formation in response to Staphylococcus aureus, J. Immunol. 185 (2010) 7413–7425.
[17] A.S. Byrd, X.M. O'Brien, C.M. Johnson, L.M. Lavigne, J.S. Reichner, An extracellular matrix-based mechanism of rapid neutrophil extracellular trap formation in response to Candida albicans, J. Immunol. 190 (2013) 4136–4148.
[18] V. Brinkmann, A. Zychlinsky, Neutrophil extracellular traps: is immunity the second function of chromatin?, J Cell Biol. 198 (2012) 773–783.
[19] A.K. Gupta, P. Hasler, W. Holzgreve, S. Gebhardt, S. Hahn, Induction of neutrophil extracellular DNA lattices by placental microparticles and IL-8 and their presence in preeclampsia, Hum. Immunol. 66 (2005) 1146–1154.
[20] R. Manzenreiter, F. Kienberger, V. Marcos, K. Schilcher, W.D. Krautgartner, A. Obermayer, M. Huml, W. Stoiber, A. Hector, M. Griese, M. Hannig, M. Studnicka, L. Vitkov, D. Hartl, Ultrastructural characterization of cystic fibrosis sputum using atomic force and scanning electron microscopy, J. Cyst. Fibros. 11 (2012) 84–92.
[21] A. Hakkim, B.G. Furnrohr, K. Amann, B. Laube, U.A. Abed, V. Brinkmann, M. Herrmann, R.E. Voll, A. Zychlinsky, Impairment of neutrophil extracellular trap degradation is associated with lupus nephritis, Proc. Natl. Acad. Sci. U.S.A. 107 (2010) 9813–9818.
[22] J. Xu, X. Zhang, R. Pelayo, M. Monestier, C.T. Ammollo, F. Semeraro, F.B. Taylor, N.L. Esmon, F. Lupu, C.T. Esmon, Extracellular histones are major mediators of death in sepsis, Nat. Med. 15 (2009) 1318–1321.
[23] A.K. Gupta, M.B. Joshi, M. Philippova, P. Erne, P. Hasler, S. Hahn, T.J. Resink, Activated endothelial cells induce neutrophil extracellular traps and are susceptible to NETosis-mediated cell death, FEBS Lett. 584 (2010) 3193–3197.
[24] D.I. Feig, D.H. Kang, R.J. Johnson, Uric acid and cardiovascular risk, N. Engl. J. Med. 359 (2008) 1811–1821.
[25] N.L. Edwards, The role of hyperuricemia in vascular disorders, Curr. Opin. Rheumatol. 21 (2009) 132–137.

PLOS ONE

CKIP-1 Is an Intrinsic Negative Regulator of T-Cell Activation through an Interaction with CARMA1

Takashi Sakamoto[1], Masayuki Kobayashi[1]*, Kohei Tada[1], Masanobu Shinohara[1], Katsuhiro Io[1], Kayoko Nagata[1], Fumie Iwai[1], Yoko Takiuchi[1], Yasuyuki Arai[1], Kouhei Yamashita[1], Keisuke Shindo[1], Norimitsu Kadowaki[1], Yoshio Koyanagi[2], Akifumi Takaori-Kondo[1]

1 Department of Hematology and Oncology, Graduate School of Medicine, Kyoto University, Kyoto, Japan, **2** Laboratory of Viral Pathogenesis, Institute for Virus Research, Kyoto University, Kyoto, Japan

Abstract

The transcription factor NF-κB plays a key regulatory role in lymphocyte activation and generation of immune response. Stimulation of T cell receptor (TCR) induces phosphorylation of CARMA1 by PKCθ, resulting in formation of CARMA1-Bcl10-MALT1 (CBM) complex at lipid rafts and subsequently leading to NF-κB activation. While many molecular events leading to NF-κB activation have been reported, it is less understood how this activation is negatively regulated. We performed a cell-based screening for negative regulators of TCR-mediated NF-κB activation, using mutagenesis and complementation cloning strategies. Here we show that casein kinase-2 interacting protein-1 (CKIP-1) suppresses PKCθ-CBM-NF-κB signaling. We found that CKIP-1 interacts with CARMA1 and competes with PKCθ for association. We further confirmed that a PH domain of CKIP-1 is required for association with CARMA1 and its inhibitory effect. CKIP-1 represses NF-κB activity in unstimulated cells, and inhibits NF-κB activation induced by stimulation with PMA or constitutively active PKCθ, but not by stimulation with TNFα. Interestingly, CKIP-1 does not inhibit NF-κB activation induced by CD3/CD28 costimulation, which caused dissociation of CKIP-1 from lipid rafts. These data suggest that CKIP-1 contributes maintenance of a resting state on NF-κB activity or prevents T cells from being activated by inadequate signaling. In conclusion, we demonstrate that CKIP-1 interacts with CARMA1 and has an inhibitory effect on PKCθ-CBM-NF-κB signaling.

Citation: Sakamoto T, Kobayashi M, Tada K, Shinohara M, Io K, et al. (2014) CKIP-1 Is an Intrinsic Negative Regulator of T-Cell Activation through an Interaction with CARMA1. PLoS ONE 9(1): e85762. doi:10.1371/journal.pone.0085762

Editor: Kjetil Tasken, University of Oslo, Norway

Received September 16, 2013; **Accepted** December 5, 2013; **Published** January 17, 2014

Funding: This work was supported by JSPS KAKENHI Grant Number 23591383. The URL is http://www.jsps.go.jp/j-grantsinaid/. The funders had no role in study design, data collection and analysis, decision to publish, or preparation of the manuscript.

Competing Interests: The authors have declared that no competing interests exist.

* E-mail: mkobayas@kuhp.kyoto-u.ac.jp

Introduction

The NF-κB family of transcription factors plays a key regulatory role in lymphocyte activation and generation of immune response [1]. The respective NF-κB target genes allow the organism to respond effectively to the environmental changes. Engagement of TCR by specific antigen presented on major histocompatibility complex (MHC) of antigen presenting cells (APC) induces T cell activation and proliferation. However, stimulation of TCR/CD3 complex alone is not sufficient for activation of NF-κB. The simultaneous costimulation of CD28 through its ligand, B7, is needed for optimal activation of NF-κB [2]. CD3/CD28 costimulation induces the formation of a large multicomponent complex at the contact site between T cell and the APC, termed as immunological synapse [3,4]. This contact area of T cells is highly enriched in cholesterol and glycosphingo-lipids, also termed as lipid rafts, and serve as the platform for the assembly of proximal signaling components of TCR. PKCθ is recruited to the immunological synapse from the cytosol upon T cell stimulation and catalytically activated [5,6]. Activated PKCθ phosphorylates CARMA1 (CARD11) to induce its conformational changes which enable CARMA1 to form the complex with Bcl10-MALT1 [7,8]. Subsequently, the IκB kinase (IKK) complex becomes activated and phosphorylates IκBs, leading to their ubiquitylation and subsequent proteasomal degradation. The degradation of IκBs allows NF-κB to enter the nucleus and induce transcription of target genes [1].

CARMA1 is one of a family of caspase recruitment domain (CARD)- and membrane associated guanylate kinase-like (MAGUK) domain-containing proteins (CARMA) [9,10]. CARMA1 contains an N-terminal CARD, followed by a coiled-coil (CC) domain, a PDZ domain, a Src homology 3 (SH3) domain, and a guanylate kinase (GUK)-like domain in the C-terminus. It has two mammalian homologs, CARMA2 and CARMA3. CARMA1 is predominantly expressed in spleen, thymus, and peripheral blood leukocyte (PBL); CARMA2 is expressed only in placenta; and CARMA3 is expressed in broad range of tissues but not in spleen, thymus or PBL. For B and T cells, the scaffold protein CARMA1 plays an essential role in antigen receptor-induced NF-κB activation [11–15]. Aberrant NF-κB activation could be involved in autoimmune diseases and malignant lymphomas. Constitutively active NF-κB in the activated B cell-like (ABC) subtype of diffuse large B cell lymphoma (DLBCL) can result from somatic mutations in genes involved in NF-κB signaling, such as CD79B, A20 and CARMA1 [16]. Recently, germline mutations in CARMA1 have also been reported in four patients with congenital B cell lymphocytosis [17]. Therefore CARMA1 activity needs to be tightly regulated.

Casein kinase-2 interacting protein-1 (CKIP-1) was originally identified as an interacting protein of casein kinase 2α (CK2α) [18]. CKIP-1 contains a pleckstrin homology (PH) domain at the N-terminus, a leucin zipper (LZ) motif at the C-terminus, and five proline-rich motifs throughout the protein [19]. Several interacting proteins of CKIP-1 have been identified and CKIP-1 plays scaffold roles in various signaling pathways [18–27]. It has also been reported that CKIP-1 binds to lipid through its PH domain and contributes to localization of its binding proteins. Genetically, CKIP-1-deficient mice show an age-dependent increase in bone mass as a result of accelerated osteogenesis, and the MEKK2-JNK-c-Jun/AP-1 axis is activated in CKIP-1 deficient mouse embryonic fibroblasts [22,25]. However, the role of CKIP-1 in NF-κB signaling remains unknown.

Many findings leading to NF-κB activation have been reported, but it is less understood how this activation is negatively regulated. To elucidate negative regulation in TCR-mediated NF-κB activation, we have done a screening by mutagenesis and complementation cloning strategies. Here we report the identification of CKIP-1 as a negative regulator in NF-κB signaling via TCR. We show that CKIP-1 interacts with CARMA1, inhibits the interaction between PKCθ and CARMA1, and suppresses NF-κB activation.

Materials and Methods

Cells

CARMA1-deficient Jurkat T cell line, named JPM50.6, and JPM50.6/WT cell line, which was reconstituted with Myc-tagged CARMA1 wild type (WT) in JPM50.6, were kindly gifted from Dr. Xin Lin [11,28]. These cell lines and Jurkat T cells were maintained with RPMI1640 (Nacalai Tesque, Kyoto, Japan) containing 10% fetal bovine serum (FBS) and 1% penicillin-streptomycin and glutamine (PSG) (Invitrogen, Carlsbad, USA). HEK293T cells were maintained with DMEM (Nacalai Tesque) containing 10% FBS and 1% PSG.

Generation of mutant Jurkat T cells and complementation cloning strategies by lentiviral cDNA library

Jurkat T cell line stably expressing EGFP under the control of an NF-κB-dependent promoter, which we called JR-GFP, was kindly gifted from Dr. Xin Lin [11]. To generate mutant cells, JR-GFP cells were treated with 4 μg/ml of ICR191 (Sigma-Aldrich, St. Louis, USA), alkylating agent that typically generates random frame-shift mutations [11,29], for 5 hr, and this treatment was repeated three times. After mutagenesis, EGFP-positive cells were sorted by BD FACSAria cell sorter (BD, New Jersey, USA) under the treatment with 2.5 μM of PKC inhibitor GF109203X (Sigma-Aldrich). Monoclonal mutant cell lines were derived by limiting dilution, and, among them, an NF-κB constitutively active cell line was identified. Human leukocyte cDNA library (Invitrogen) on pCS2-EF-GATEWAY-IRES-hrGFP was transferred into pCS2-EF-GATEWAY-IRES-$H2K^k$ through LR reaction on Gateway cloning system (Invitrogen) and cDNA and $H2K^k$-dual expressing lentiviral vector were prepared as described before [30,31]. To identify NF-κB negative regulators, the NF-κB constitutively active cell line was infected with this viral vector. If the mutant phenotype was rescued by the gene from the library, EGFP expression might return to negative. Both $H2K^k$-positive and EGFP-negative cells were sorted using BD FACSAria cell sorter and subjected to limiting dilution. If EGFP was normally induced by PMA/ionomycin in each single cell clone, the mutant phenotype should be rescued by the gene from the library. The genes rendering the reversion of the mutant phenotype were isolated by PCR using vector specific primers. Subsequent DNA sequencing and BLAST analysis should reveal the integrated gene.

Plasmid constructs

Plasmids encoding Myc-CARMA1, Myc-CARMA1 truncated forms, EGFP-CARMA1, Myc-Bcl10, PKCθ WT, PKCθ AE [32], IKKβ, and GFP-NF-κB RelA were kind gifts from Dr. Xin Lin. Expression vectors for FLAG-CARMA1 and HA-Bcl10 were generated by subcloning of coding sequence into pcDNA3 vector (Invitrogen). GST-CARMA1 CD-CC was generated by subcloning of coding sequence into pGEX-4T-1 (GE Healthcare, Buckinghamshire, UK). Human CKIP-1 cDNA was generated by PCR amplification from Jurkat cDNA and cloned into pcDNA3/hygro and pcDNA3-FLAG vector (Invitrogen). Expression vector for DsRed-CKIP-1 was generated by subcloning of coding sequence into pDsRed1-N1 vector (Clontech, Mountain View, USA). ΔLZ-CKIP-1 and ΔPH-CKIP-1 truncated form were generated by PCR amplification from WT CKIP-1 expression vector and subcloned into pcDNA3/hygro vector.

RNA interference

To identify a negative signaling component of NF-κB signaling from our candidates, we knocked down the molecules by specific siRNA in JR-GFP cells. siRNAs against our selected eighteen candidates were purchased from Thermo Scientific (Rockford, USA) (siGENOME SMARTpool). 5×10^6 JR-GFP cells were electroporated with 400 pmol of non-targeting siRNA (D-001206-13), human TNFAIP3 (A20)-specific siRNA (M-009919-00), human CKIP-1-specific siRNA (M-016800-01), and siRNAs against other seventeen genes using AMAXA Nucleofector System (Lonza, Basel, Switzerland). Five days later, EGFP expression was analyzed by BD FACSCalibur. siRNA SMARTpool (Thermo Scientific) is a mixture of four siRNAs. We also used separate aliquot of four individual siRNAs (D-016800-01, 02, 03, 04).

Chemicals, Cytokines, and Antibodies

PMA and ionomycin were purchased from Sigma-Aldrich. TNFα was from CellGenix (Freiburg, Germany). PE-conjugated anti-mouse $H2K^k$ (CL9005PE) was from Cedarlane (Ontario, Canada). Anti-GFP (A6455) was from Molecular Probes (Eugene, USA). Mouse anti-human CD3 (555336), -CD28 (555725), and -PKCθ (610089) were from BD Biosciences (San Jose, USA). Anti-CKIP-1 (D-20, sc-50225), -IKKα/β (H470, sc-7607), and -Lck (3A5, sc-433) were from Santa Cruz Biotechnology (Santa Cruz, USA). Anti-β-actin (AC-15, A5441), -c-Myc (9E10, M5546, and C3956), and -FLAG (M2, F3165) were from Sigma-Aldrich. Anti-HA (12CA5) was from Roche (Mannheim, Germany). Anti-p-Erk (Thr202/Tyr204, E10, #9106), -Erk (#9102), and -CARMA1 (1D12, #4435) were from Cell Signaling Technology (Danvers, USA).

Luciferase reporter assay

5 μg of 5xNF-κB-dependent luciferase (*Firefly*) reporter plasmid and 0.1 μg of EF1α promoter-dependent *Renilla* luciferase reporter were transfected together with 5 μg of plasmids encoding the desired genes or 400 pmol of siRNA by electroporation into 1×10^7 Jurkat T cells in 0.4 ml serum-free RPMI1640 media at the power setting of 250 V and 950 μF. Nineteen hours later, the transfected cells were treated for 5 hr with plate-bound CD3 mAb (2 μg/ml), plate-bound CD3 + soluble CD28 mAb (2 μg/ml of each), TNFα (20 ng/ml), PMA (10 ng/ml), or PMA (10 ng/ml) + CD28 (2 μg/ml). NF-κB activity was measured with Dual-

Luciferase Reporter Assay System (Promega, Madison, USA) and was determined by normalization of NF-κB-dependent *Firefly* luciferase to *Renilla* luciferase activity. Values represent the average of three independent experiments and error bars represent the SD from the average. Statistically significance was determined using Student's t test.

Evaluation of NF-κB activity

Nuclear protein fractions were harvested by the Nuclear Extract kit (Active Motif, Carlsbad, USA). NF-κB activity was measured in 2 μg of nuclear protein extracts by the TransAM^{TM} NF-κB p65 chemi (Active Motif), an ELISA-based kit to detect and quantify NF-κB p65 subunit activation. The assay was performed according to the manufacturer's protocol and analyzed using a microplate luminometer PerkinElmer 2030 ARVO^{TM} X3 (PerkinElmer, Waltham, USA). Values represent the average of three independent experiments and error bars represent the SD from the average. Statistically significance was determined using Student's t test.

Immunoprecipitation

For co-immunoprecipitation, 6-well plate HEK293T cells were transfected by the calcium phosphate method. Two days after transfection, cells were lysed in NP-40 lysis buffer (20 mM Tris-HCl pH 7.5, 250 mM NaCl, 1% NP-40) supplemented with 1 mM PMSF, protease inhibitor cocktail (Nacalai Tesque) and phosphatase inhibitor cocktail (Roche). Total cell lysates were precleared on Protein A Sepharose beads for 30 min at 4°C. The precleared cell lysates were immunoprecipitated with Protein A beads-conjugated with the desired antibodies for 6 hr. Immunoprecipitates were washed three times with lysis buffer.

To detect the protein interaction in JPM50.6/WT cells, 1×10^8 cells were lysed in NP-40 lysis buffer (10 mM Tris-HCl pH 7.5, 150 mM NaCl, 0.5% NP-40) supplemented with protease inhibitor cocktail (Nacalai Tesque) and phosphatase inhibitor cocktail (Roche). Total cell lysates were precleared on Protein A Sepharose beads for 30 min at 4°C. The precleared cell lysates were immunoprecipitated with Protein A beads-conjugated with 2 μg of anti-CKIP-1 Ab at 4°C overnight. Immunoprecipitates were washed three times with 0.05% NP-40 buffer (10 mM Tris-HCl pH 7.5, 150 mM NaCl, 0.05% NP-40).

Confocal microscopy

HEK293T cells were transfected with expression vectors and grown on the coverslips. 24 hr after transfection, the cells were incubated with Alexa Flour 488-conjugated cholera toxin B (Molecular probes) at 4°C for 20 min. The specimens were fixed with 4% paraformaldehyde in PBS and mounted on slides using ProLong Gold antifade reagent with DAPI (Invitrogen), and analyzed by confocal laser scanning fluorescence microscopy (Nikon Digital Eclipse C1).

In vitro binding assay

FLAG-CKIP-1 was synthesized *in vitro* using the TNT T7 Quick Coupled Transcription/Translation System (Promega). GST and GST-CARMA1 CD-CC proteins were produced in *E. coli* BL21 and purified with glutathione Sepharose 4B beads (GE Healthcare). The beads were incubated with FLAG-CKIP-1 at 4°C for 2 hr. The beads were washed and proteins were eluted, followed by Western blotting with anti-FLAG antibody.

Lipid raft purification

Costimulation of Jurkat T cells was performed in a final volume of 1 ml by addition of anti-CD3 (10 μg/ml) and anti-CD28 (5 μg/ml) antibodies, together with 15 μg of mouse IgG (Sigma-Aldrich). Cells (2×10^7) were lysed in 1 ml MNE Buffer (25 mM MES pH 6.5, 150 mM NaCl, 5 mM EDTA) with 1% Triton-X, 1 mM PMSF, and protease inhibitor cocktail (Nacalai Tesque) for 20 min on ice and dounce homogenized 20 times. Samples were centrifuged at 1,000× g for 10 min at 4°C. The supernatants were mixed with 1 ml of OptiPrep (Axis-Shield, Oslo, Norway) and transferred to a Beckman Ultracentrifuge tube. Two milliliters of 30% OptiPrep followed by 1 ml of 5% OptiPrep in MNE buffer were overlaid. Samples were ultracentrifuged in a SW41Ti rotor (200,000× g for 20 hr). Fractions (400 μl per fraction) were collected from the top of the gradient. Proteins from each fraction were precipitated with trichloroacetic acid before separation by SDS-PAGE and Western blotting.

Results

Identification of CKIP-1 as a negative regulator of NF-κB activation

We have performed a cell-based screening to find negative regulators in TCR-mediated NF-κB activation, using somatic mutagenesis and complementation cloning strategies [11,29]. We used Jurkat T cell line expressing EGFP under the control of an NF-κB-dependent promoter, named JR-GFP [11]. To generate NF-κB constitutively active cell lines, JR-GFP cells were subjected to mutagenesis with ICR191, and EGFP-positive cells were sorted under the treatment of PKC inhibitor GF109203X. After limiting dilution, we identified an NF-κB constitutively active cell line in which negative regulators for NF-κB activation must be mutated. To identify NF-κB negative regulators, the NF-κB constitutively active cell line was infected with a human leukocyte-cDNA library expressing lentivirus, and EGFP-negative cells were sorted. If the mutant phenotype was rescued by transduction of the gene from the library, EGFP expression would return to negative. The genes rendering the reversion of the mutant phenotype were isolated by PCR and sequenced using library vector specific primers, and then we obtained dozens of candidates for NF-κB negative regulators. To examine whether any of these candidates downregulate NF-κB activity, we selected and knocked down eighteen molecules by specific siRNA in JR-GFP cells. We found that knockdown of CKIP-1 induced expression of EGFP more than that of TNFAIP3 (A20), which was known as a negative regulator of NF-κB and used as a positive control [33] (Figure S1). To confirm that CKIP-1 was a negative regulator of NF-κB, Jurkat T cells were transfected with CKIP-1 siRNA together with an NF-κB-dependent luciferase reporter plasmid. We used siRNA SMARTpool, which is a mixture of four siRNAs, and separate aliquot of all four individual siRNAs. Knockdown of CKIP-1 increased NF-κB activity (Figure 1A). We also showed that knockdown of CKIP-1 induced DNA binding activity of NF-κB p65 (Figure 1B), by using the transcription factor DNA-binding ELISA. Thus, we clearly demonstrated that CKIP-1 was a novel NF-κB negative regulator.

CKIP-1 suppresses NF-κB activation induced by PMA and constitutively active PKCθ

To examine whether the downregulation of NF-κB activation by CKIP-1 is specific to TCR stimulation, Jurkat T cells transfected with CKIP-1, treated with different stimulation, and assessed NF-κB activity by luciferase reporter assays. CKIP-1 suppressed NF-κB activity in unstimulated cells and stimulated by CD3, PMA and PMA/CD28, but not by TNFα or CD3/CD28

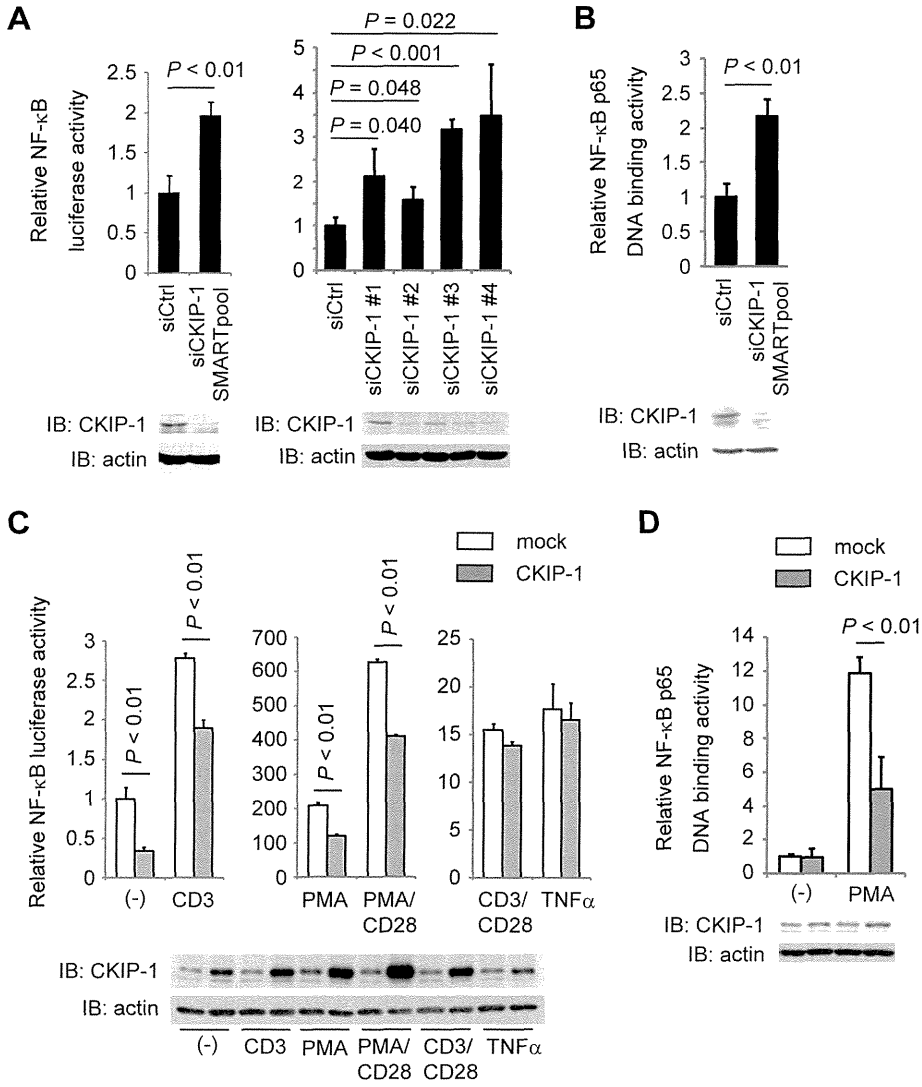

Figure 1. Identification of CKIP-1 as a negative regulator in NF-κB activation. (A) 400 pmol of human CKIP-1-specific siRNA or non-targeting siRNA together with 5 μg of κB-Luc, 0.1 μg of *Renilla*-Luc were electroporated into Jurkat T cells. Luciferase activity was assayed after 48 hr. The reduction of endogenous CKIP-1 protein levels was analyzed by Western blotting. (B) Jurkat T cells were electroporated with human CKIP-1-specific siRNA or non-targeting siRNA using AMAXA Nucleofector System (Lonza). Thirty hours later, nuclear protein extracts were harvested and NF-κB activity was measured by TransAM NF-κB p65 chemi kit (Active Motif). The reduction of endogenous CKIP-1 protein levels was analyzed by Western blotting. (C) Jurkat T cells were transfected with 5 μg of CKIP-1 or empty vector (mock) together with 5 μg of κB-Luc and 0.1 μg of *Renilla*-Luc. Nineteen hours later, cells were stimulated for 5 hr upon CD3 (2 μg/ml), CD3/CD28 (2 μg/ml each), TNFα (20 ng/ml), PMA (10 ng/ml) or PMA (10 ng/ml) + CD28 (2 μg/ml). The expressed protein levels were analyzed by Western blotting. (D) Jurkat T cells were transfected with 5 μg of CKIP-1 or empty vector (mock). Twenty-four hours later, cells were stimulated for 30 min upon PMA (10 ng/ml). Then cells were harvested and NF-κB activity was measured by TransAM NF-κB p65 chemi kit. The expressed protein levels were analyzed by Western blotting. Values represent the average of three independent experiments and error bars represent the SD from the average.
doi:10.1371/journal.pone.0085762.g001

(Figure 1C). Using the transcription factor DNA-binding ELISA, we also showed that CKIP-1 suppressed NF-κB activation induced by PMA stimulation (Figure 1D). These data suggest that CKIP-1 inhibits NF-κB signaling via TCR but not via TNF receptor and that CKIP-1 targets downstream signaling components of PKCθ, since the treatment of PMA directly activates PKCs. To clarify which step of signaling CKIP-1 affects, NF-κB activation driven by transfection of each downstream signaling component of PKCθ was assessed in Jurkat T cells in the presence or absence of co-transfection of CKIP-1 (Figure 2A). NF-κB activation induced by PKCθ AE, a constitutively active mutant [32], was clearly suppressed by CKIP-1, whereas activation induced by NF-κB RelA, IKKβ or Bcl10 was not affected. NF-κB activation induced by CARMA1 seemed to be suppressed by CKIP-1, but the effect was not statistically significant. Conversely, knockdown of CKIP-1 increased NF-κB activation induced by transfection of CARMA1 or PKCθ AE (Figure 2B). These results suggest that the inhibitory effect of CKIP-1 targets signaling events around PKCθ or CARMA1.

As shown in Figure 1C, CKIP-1 did not suppress CD3/CD28-induced NF-κB activation. We hypothesized that CKIP-1 might work in a resting state and finish its role during CD3/CD28 costimulation. PKCθ and CARMA1 have been reported to be recruited to lipid rafts upon TCR stimulation [34]. It has been

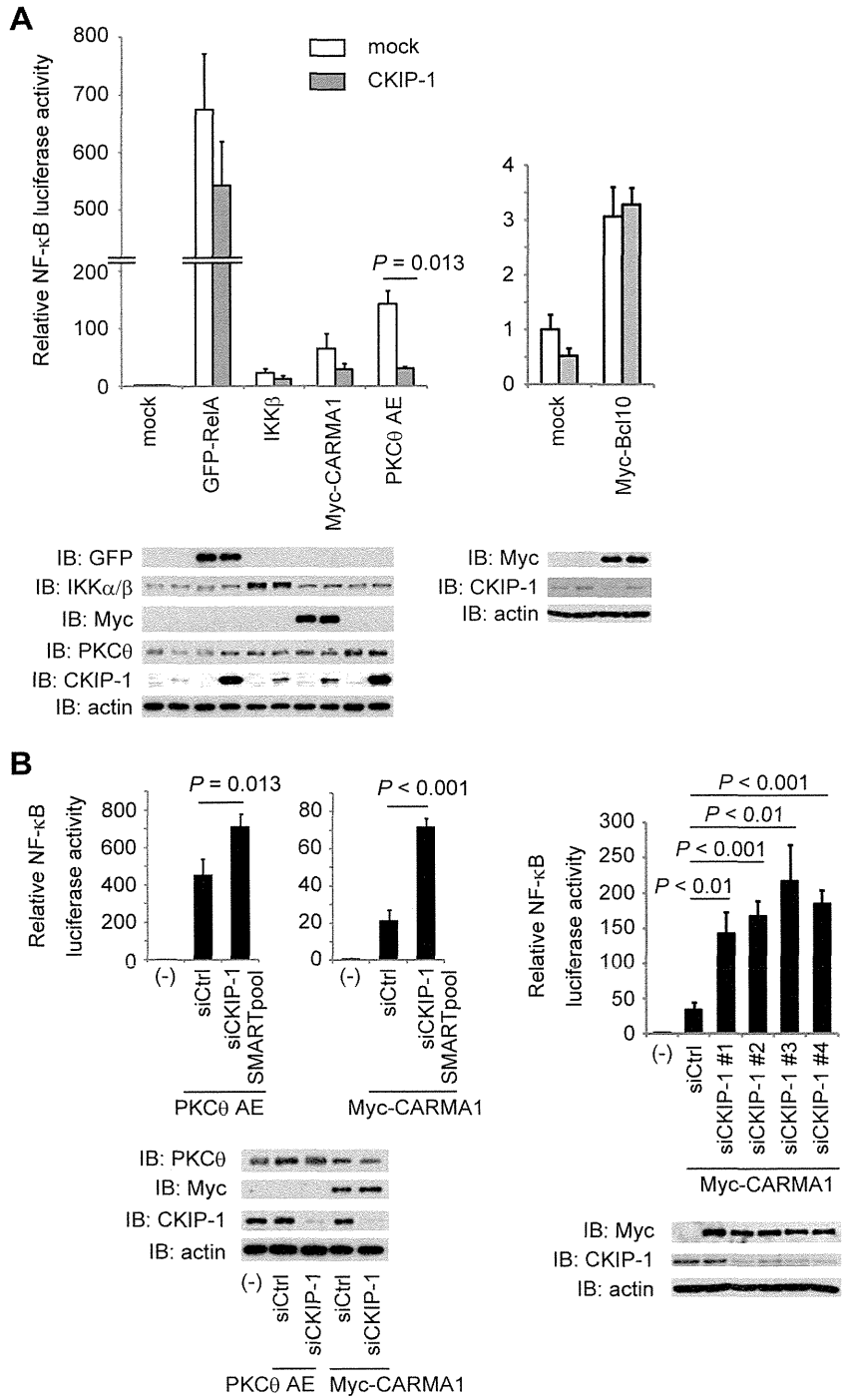

Figure 2. CKIP-1 suppresses NF-κB activation induced by constitutively active PKCθ. (A) Jurkat T cells were transfected with 5 μg of CKIP-1 or empty vector (mock) together with 5 μg of each signaling component, 5 μg of κB-Luc and 0.1 μg of *Renilla*-Luc by electroporation. Luciferase activity was assayed after 24 hr. PKCθ AE is constitutively active mutant. The expressed protein levels were analyzed by Western blotting. (B) Jurkat T cells were transfected with 400 pmol of human CKIP-1-specific siRNA or non-targeting siRNA together with 5 μg of κB-Luc, 0.1 μg of *Renilla*-Luc, and 5 μg of PKCθ AE (left panel) or CARMA1 (right panel) by electroporation. Thirty hours later, cells were lysed and luciferase activity was assayed. The expressed protein levels were analyzed by Western blotting. Values represent the average of three independent experiments and error bars represent the SD from the average.
doi:10.1371/journal.pone.0085762.g002

shown that CKIP-1 binds to lipid through its PH domain and overexpressed CKIP-1 localizes in the plasma membrane and partly in the nucleus [18,20,22]. To examine where CKIP-1 localizes in Jurkat T cells, the detergent-insoluble membrane (lipid raft) fractions were prepared by the ultra-centrifugation in a discontinuous OptiPrep density gradient. Lck was constitutively associated with lipid rafts, and PKCθ was recruited to lipid rafts after CD3/CD28 costimulation (Figure 3) as previously reported

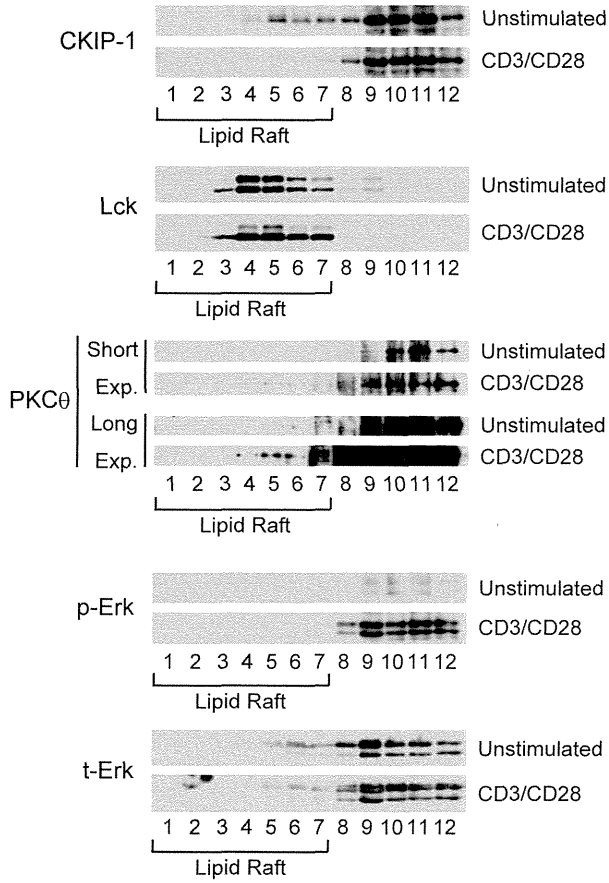

Figure 3. Lipid rafts accumulated by CD3/CD28 costimulation do not contain CKIP-1. Jurkat T cells were stimulated for 15 min with anti-CD3 (10 μg/ml) and anti-CD28 (5 μg/ml), together with 15 μg of mouse IgG. The cells were then lysed and subjected to OptiPrep density gradient centrifugation to isolate lipid rafts. Lysates were subjected to SDS-PAGE and analyzed by Western blotting.
doi:10.1371/journal.pone.0085762.g003

[28,35]. Phosphorylation of Erk was induced by CD3/CD28 costimulation. CKIP-1 partly localized at lipid rafts in unstimulated Jurkat T cells, and intriguingly, CKIP-1 was excluded from lipid rafts when cells were stimulated upon CD3/CD28 (Figure 3). These data suggest that, when cells are stimulated upon CD3/CD28 and lipid rafts are accumulated, CKIP-1 localizes out of the lipid rafts and its inhibitory effect does not extend.

Identification of CARMA1 as a binding partner of CKIP-1

To determine the interacting partner of CKIP-1, we examined whether CKIP-1 associates with PKCθ or CARMA1 by co-immunoprecipitation assays in HEK293T cells. CKIP-1 interacted with Myc-CARMA1 but not with PKCθ (Figure 4A, lane 1–4, Figure 4B, lane 1 and 2). In the presence of co-transfection of PKCθ, CKIP-1 also interacts with Myc-CARMA1 (Figure 4A, lane 5 and 6, Figure 4B, lane 3 and 4). We examined CKIP-1 and CARMA1 localization in HEK293T cells by confocal microscopy. HEK293T cells were transfected with DsRed-CKIP-1 and EGFP-CARMA1. The lipid rafts of transfected cells were stained with Alexa Flour 488-conjugated cholera toxin B (CTx). DsRed-CKIP-1 colocalized with Alexa Flour 488-CTx-labeled lipid rafts (Figure 4C, upper panel), and colocalized extensively with EGFP-CARMA1 (Figure 4C, lower panel). This result indicates that CKIP-1 colocalizes with CARMA1 at the plasma membrane.

Next, we examined the interaction between CKIP-1 and CARMA1 in T cells, using JPM50.6/WT cells, which were reconstituted with Myc-CARMA1 wild type (WT) in CARMA1-deficient Jurkat (JPM50.6) T cells [11,28]. Myc-CARMA1 was co-immunoprecipitated with endogenous CKIP-1 but not with control IgG (Figure 4D). To determine the domain of CARMA1 that was critical for the interaction with CKIP-1, truncated forms of CARMA1 were tested (Figure 4E). Co-immunoprecipitation assays showed that CKIP-1 bound to CARMA1 WT, CD-CC and ΔCD, but not to ΔCD-CC (Figure 4F), indicating that CKIP-1 associates with the CC domain of CARMA1. To determine the responsible region in CKIP-1 for the association with CARMA1, we generated several CKIP-1 truncated forms (Figure 4E). Co-immunoprecipitation assays revealed that CKIP-1 WT and ΔLZ bound to CARMA1 but CKIP-1 ΔPH did not (Figure 4G), indicating that the PH domain of CKIP-1 was essential for the interaction with CARMA1. To investigate direct interaction between CKIP-1 and CARMA1, *in vitro* GST pull-down assay was performed. GST-tagged CARMA1 CD-CC was able to interact with FLAG-CKIP-1 but GST was not (Figure 4H). Together, CARMA1 is a specific interacting partner of CKIP-1.

PH domain of CKIP-1 is essential for the interaction with CARMA1 and the inhibitory effect on NF-κB activation

Next we examined the function of each truncated form of CKIP-1 on NF-κB activation, using luciferase reporter assays. Jurkat T cells were transfected with each CKIP-1 truncated form and stimulated by PMA and CD3/CD28. CKIP-1 WT and ΔLZ inhibited NF-κB activation induced by stimulation with PMA, but CKIP-1 ΔPH did not (Figure 5A, middle panel). Similarly to CKIP-1 WT (Figure 1C), the truncated forms of CKIP-1 gave no influence upon CD3/CD28-induced-NF-κB activation (Figure 5A, right panel). In resting state, the effect of the truncated forms was not statistically significant, because of the little amount of NF-κB activity in unstimulated cells (Figure 5A, left panel). Jurkat T cells were transfected with PKCθ AE together with each CKIP-1 truncated form. CKIP-1 WT and ΔLZ suppressed NF-κB activation, but CKIP-1 ΔPH did not (Figure 5B, left panel). As shown in Figure 2A, NF-κB activation induced by CARMA1 seemed to be suppressed by CKIP-1 WT, but the effect was not statistically significant. Neither CKIP-1 ΔLZ nor ΔPH repressed NF-κB activation induced by CARMA1 (Figure 5B, right panel). These results suggest that PH domain of CKIP-1, which is required for association with CARMA1, is essential for the inhibitory effect on NF-κB activation.

CKIP-1 inhibits the interaction between PKCθ and CARMA1

PKCθ phosphorylates CARMA1 in its Linker between the CD-CC domain and the MAGUK domain, which induces conformational change of CARMA1 [7,8]. Then CARMA1 binds to Bcl10 through CARD-CARD interaction [9,36]. Since our data suggested that CKIP-1 interacted with the CC domain of CARMA1, we hypothesized that CKIP-1 might inhibit the interaction between CARMA1 and PKCθ or between CARMA1 and Bcl10. Co-immunoprecipitation assays showed that CKIP-1 inhibited the interaction between PKCθ and CARMA1, but not that between CARMA1 and Bcl10 (Figure 6A). As shown in Figure 4B (lane 5 and 6), PKCθ was immunoprecipitated with Myc-CARMA1, but, in the presence of co-transfection of CKIP-1, the interaction between PKCθ and CARMA1 was diminished (Figure 4B, lane 3 and 4). Next, we examined the inhibitory effect of CKIP-1 truncated forms on the interaction between PKCθ and

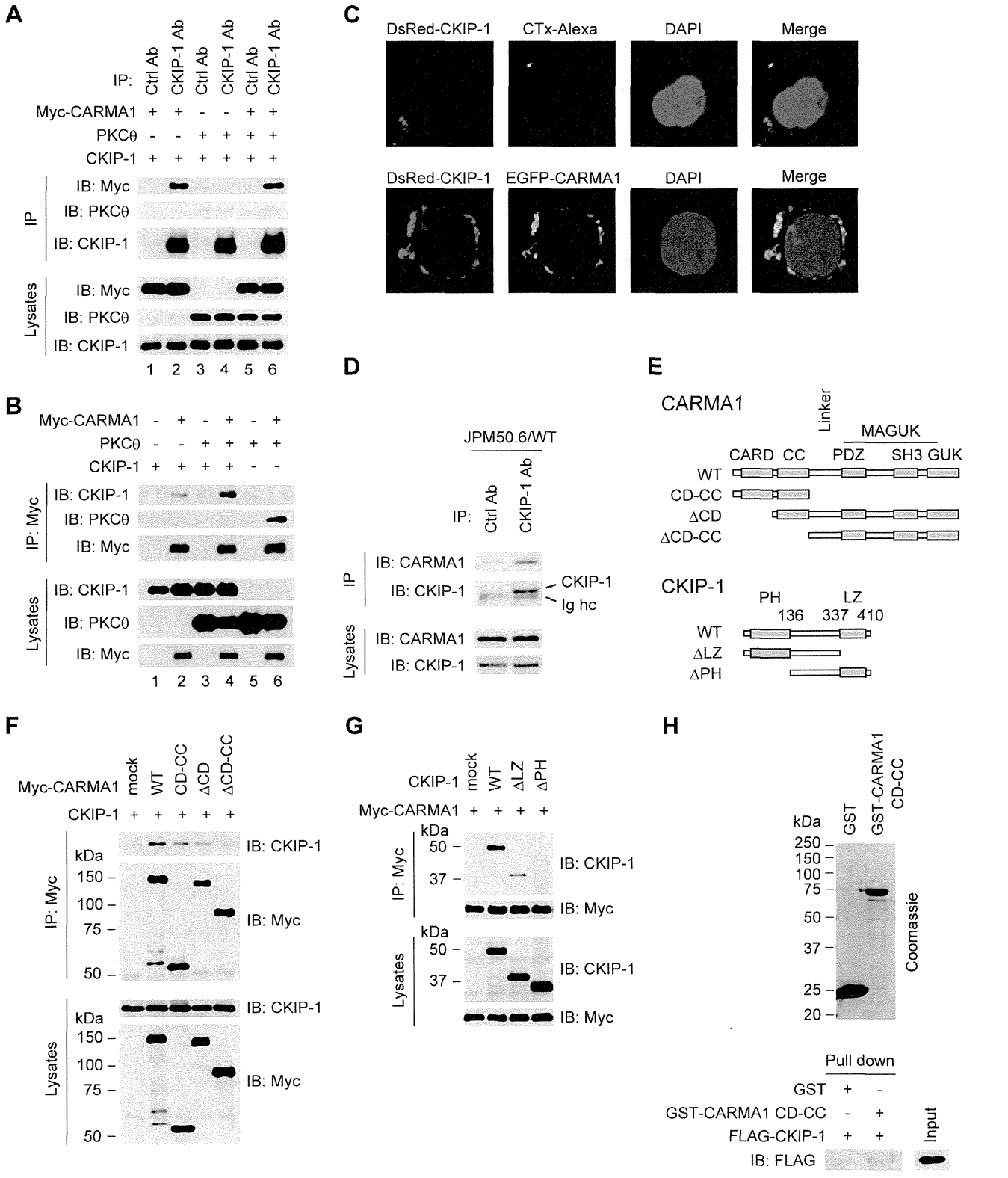

Figure 4. Identification of CARMA1 as a binding partner of CKIP-1. (A) HEK293T cells were transfected with plasmids encoding CKIP-1 together with Myc-CARMA1 or PKCθ, lysed, and immunoprecipitated by anti-CKIP-1 or control antibody. (B) HEK293T cells were co-transfected with plasmids encoding Myc-CARMA1, PKCθ or CKIP-1, lysed, and immunoprecipitated by anti-Myc antibodies. (C) HEK293T cells were transfected with DsRed-CKIP-1. 24 hr later, the transfected cells were incubated with Alexa Flour 488-conjugated cholera toxin B (CTx), and were fixed and stained with DAPI. In lower panels, HEK293T cells were transfected with DsRed-CKIP-1 together with EGFP-CARMA1. 24 hr later, cells were fixed and stained with DAPI. The localization of CKIP-1, CARMA1 and Alexa Flour 488-CTx-labeled lipid rafts was visualized by confocal microscopy. (D) JPM50.6/WT cells, which were reconstituted by Myc-CARMA1 WT into CARMA1-deficient Jurkat T cells, were lysed and immunoprecipitated by anti-CKIP-1 or control antibody. Ig hc, immunoglobulin heavy chain. (E) Schematic diagram of CARMA1 and CKIP-1 truncated forms used in the experiments. CARD,

caspase recruitment domain; CC, coiled-coil; SH3, Src homology 3; GUK, guanylate kinase; MAGUK, membrane-associated GUK; PH, pleckstrin homology; LZ, leucin zipper. (F) HEK293T cells were transfected with CKIP-1 together with Myc-CARMA1 truncated form, lysed, and immunoprecipitated by anti-Myc antibody, followed by Western blotting with indicated antibodies. (G) HEK293T cells were transfected with Myc-CARMA1 together with each CKIP-1 truncated form. Cell lysates were immunoprecipitated by anti-Myc antibody, followed by Western blotting with indicated antibodies. (H) CARMA1 CD-CC was purified from *E. coli* as a GST fusion protein. GST alone or GST-tagged CARMA1 CD-CC was incubated with *in vitro* transcribed/translated FLAG-CKIP-1. GST pull-downs and input were subjected to Western blotting with anti-FLAG antibody.
doi:10.1371/journal.pone.0085762.g004

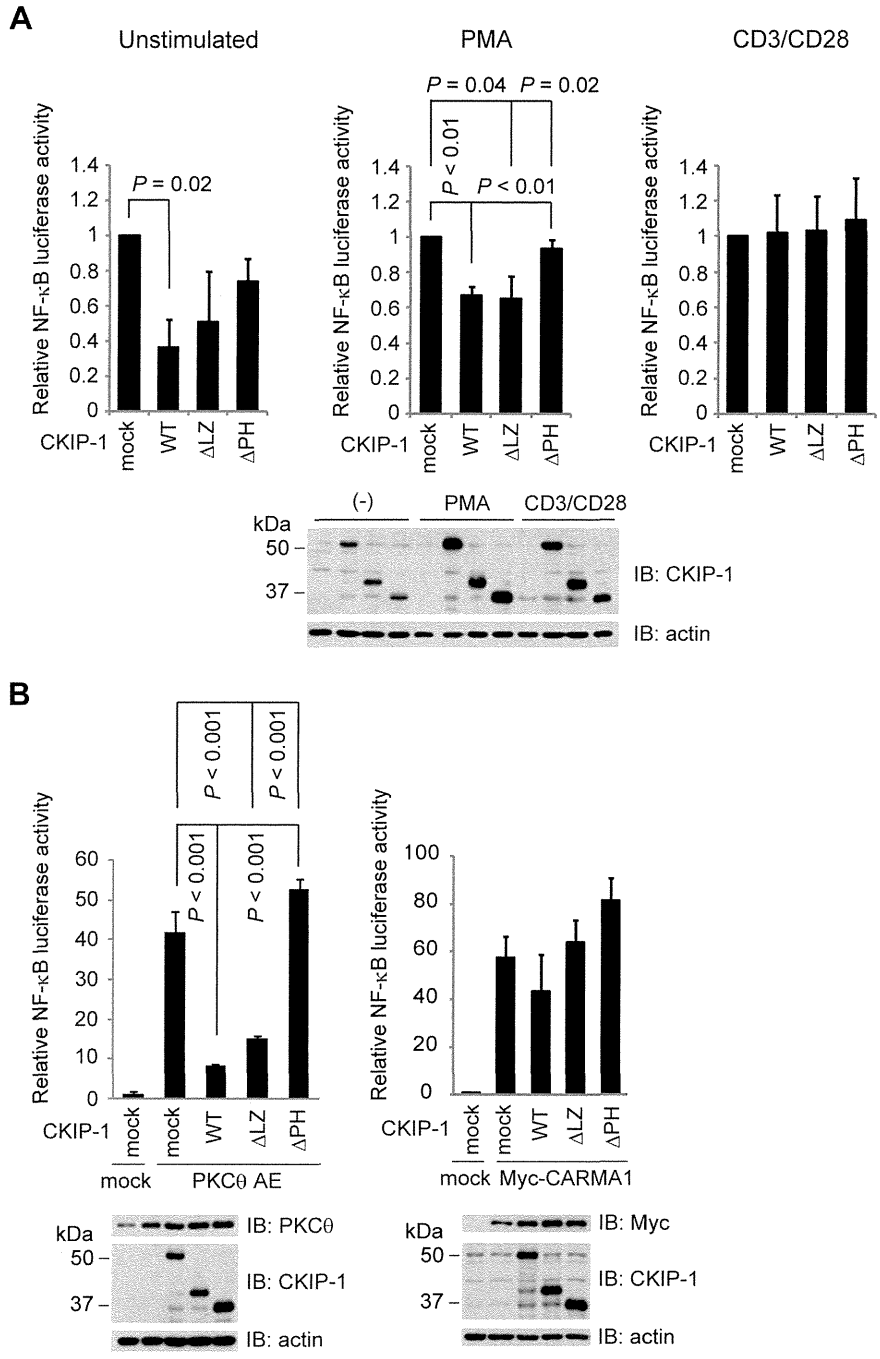

Figure 5. PH domain of CKIP-1 is essential not only for the interaction with CARMA1 but also for the inhibitory effect on NF-κB activation. (A) Jurkat T cells were electroporated with 5 μg of each CKIP-1 truncated form together with 5 μg of κB-Luc and 0.1 μg of *Renilla*-Luc. Nineteen hours later, cells were stimulated for 5 hr upon PMA (10 ng/ml) or CD3/CD28 (2 μg/ml each). The expressed protein levels were analyzed by Western blotting. (B) Jurkat T cells were electroporated with 5 μg of each CKIP-1 truncated form together with 5 μg of PKCθ AE or Myc-CARMA1, 5 μg of κB-Luc and 0.1 μg of *Renilla*-Luc. After 24 hr, cells were lysed and luciferase activity was assessed. The expressed protein levels were analyzed by Western blotting. Values represent the average of three independent experiments and error bars represent the SD from the average.
doi:10.1371/journal.pone.0085762.g005

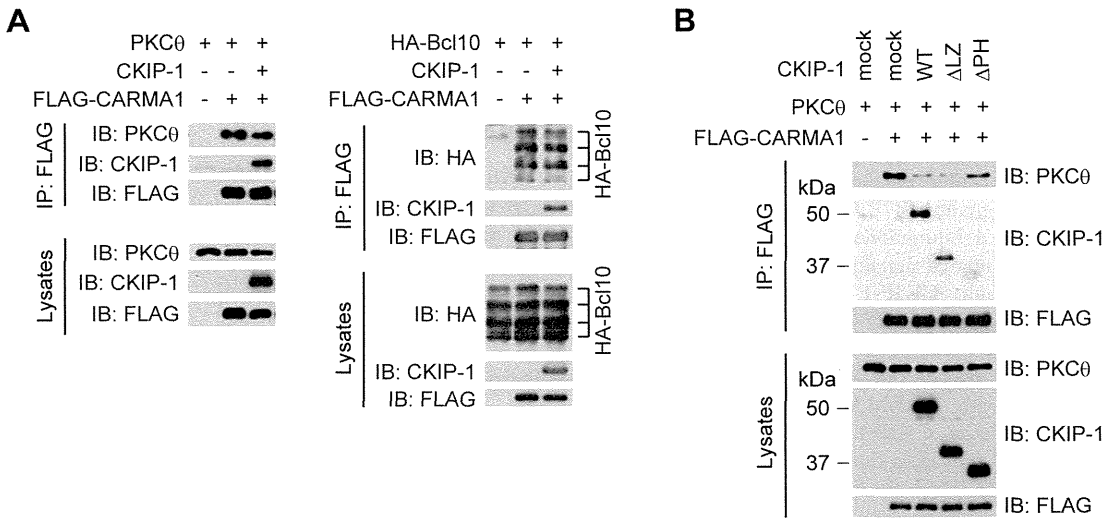

Figure 6. CKIP-1 inhibits the interaction between PKCθ and CARMA1. (A) HEK293T cells were transfected with CKIP-1 or empty vector (mock) together with PKCθ and FLAG-CARMA1 (left panel), or together with HA-Bcl10 and FLAG-CARMA1 (right panel). Cell lysates were immunoprecipitated by anti-FLAG antibody, followed by Western blotting with indicated antibodies. (B) HEK293T cells were transfected with CKIP-1 truncated form together with PKCθ and FLAG-CARMA1. Cell lysates were immunoprecipitated by anti-FLAG antibody, followed by Western blotting with indicated antibodies.
doi:10.1371/journal.pone.0085762.g006

CARMA1. Consistent with the results of the binding and the inhibitory effect of the truncated forms (Figure 4G and Figure 5), CKIP-1 WT and ΔLZ inhibited the interaction between PKCθ and CARMA1, although CKIP-1 ΔPH showed no effect (Figure 6B). These results suggest that CKIP-1 suppresses NF-κB activation by inhibiting the interaction between PKCθ and CARMA1.

Discussion

NF-κB signaling in antigen-stimulated lymphocytes plays an important role in immune response. Aberrant NF-κB activation has been shown to be involved in autoimmune diseases and malignant lymphomas. Especially, altered expression and/or function of CBM proteins have been reported in the ABC subtype of DLBCL [16,37,38] and MALT lymphoma [39].

In this study, we show that CKIP-1 is a novel interacting protein with CARMA1 and acts as a suppressor of NF-κB signaling. Our results suggest that CKIP-1 suppresses NF-κB signaling by inhibiting the interaction between PKCθ and CARMA1. However, CKIP-1 does not suppress NF-κB activation induced by CD3/CD28 costimulation. Our data suggest that it is because CKIP-1 localizes outside of the lipid rafts and its inhibitory effect does not extend, when cells are stimulated upon CD3/CD28 and lipid rafts are accumulated. A transmembrane adaptor molecule PAG/Cbp is also a negative regulator of T cell activation. In resting T cells, PAG/Cbp is phosphorylated by Lck and interacts with C-terminal Src kinase (Csk), which inhibits T cell activation by suppressing c-Src. In response to stimulation of TCR, PAG/Cbp becomes rapidly dephosphorylated and dissociates from Csk [40,41]. Likewise, IκBs usually retain NF-κB in the cytoplasm through physical interaction. In response to signaling, IκBs are phosphorylated, leading to their ubiquitylation and subsequent proteasomal degradation [42]. Similarly to PAG/Cbp or IκBs, CKIP-1 usually interacts with CARMA1, but its inhibitory effect might be abrogated during CD3/CD28 costimulation. We presume that CKIP-1 physiologically prevents T cells from being activated by inadequate stimulation and might play a role like a gatekeeper for correct CD3/CD28 signaling at the step of CARMA1 during antigen-stimulation. We speculate that, in resting T cells, CKIP-1 associates with CARMA1 and keeps PKCθ away from CARMA1. Our date clearly showed that when T cells are stimulated appropriately upon CD3/CD28 costimulation, both PKCθ and CARMA1 are recruited to lipid rafts. However, CKIP-1 remains outside of the lipid rafts, and its inhibitory effect cannot extend. CARMA1 is then phosphorylated by PKCθ at the lipid rafts leading to its conformational change into an active form. The activated CARMA1 recruits Bcl10-MALT1 complex and subsequently induces NF-κB activation.

PAG/Cbp-deficient mice exhibit no overt phenotype [43,44], but, in cancer cells, PAG/Cbp is involved in repressing the oncogenecity of c-Src [45]. CKIP-1-deficient mice are reported to undergo an age-dependent increase in bone mass [25]. However, no phenotype about immune disorders or neoplasm has been described. Thus, PAG/Cbp and CKIP-1 might be dispensable or could be compensated by some other negative regulators, because multiple checkpoints through TCR-mediated NF-κB signaling are likely to be independently required to prevent the unwarranted expansion and transformation of lymphocytes, and to ensure an appropriate adaptive immune response. Our data suggest that the suppression of CKIP-1 can work in a resting state or against aberrant PKCθ activation such as expression of constitutively active PKCθ or treatment of PMA. Similarly to PAG/Cbp, only in malignant lymphomas or immunological disorders, CKIP-1 might play a critical role as a suppressor of aberrant NF-κB activation.

Recently, novel germline CARMA1 mutations have been reported in four patients with congenital B cell lymphocytosis [17]. These CARMA1 mutants constitutively drive NF-κB activation, resulting in elevated NF-κB activity and increased proliferation of patient primary B cells. However, patient primary T cells expressing these CARMA1 mutants are hyporesponsive to CD3/CD28 costimulation. It has also been reported that chronic NF-κB activation, triggered by transgenic expression of constitutively active IKKβ in mice, renders T cells hyporesponsive to TCR stimulation [46]. We speculate that T cells have the mechanism by which an anergic state is induced by chronic active

NF-κB signaling, and it might be one of the reasons why knockdown of CKIP-1 did not exhibit clear phenotypes in TCR stimulation. Analysis of B cells might be useful for deciphering the physiological role of CKIP-1.

There have been already reported two inhibitory regulators that interact with CARMA1. The kinesin GAKIN negatively regulates occupancy of CARMA1 at the center of the immunological synapse, and limits the extent of signaling [47]. Casein kinase 1α (CK1α), which is reported to be a bifunctional regulator, also interacts with CARMA1 and terminates signaling by phosphorylating CARMA1 [48]. Although CKIP-1 interacts with CARMA1 as GAKIN and CK1α do, CKIP-1 shows several different aspects. Whereas GAKIN competes with Bcl10 for binding, CKIP-1 competes with PKCθ but not with Bcl10. GAKIN and CK1α associate with CARMA1 in a signal-dependent manner. On the other hand, CKIP-1 neither localizes at lipid rafts nor influences NF-κB activation during CD3/CD28 costimulation. To our knowledge, CKIP-1 is the first molecule that negatively regulates CARMA1 in a resting state or in aberrantly activated signaling.

In conclusion, we have herein demonstrated an inhibitory effect of CKIP-1 in PKCθ-CBM-NF-κB signaling. CKIP-1 interacts with CARMA1 and competes with PKCθ for binding. It suggests that CKIP-1 plays a unique role to keep resting T cells in a quiescent state or to prevent T cells from being activated by inadequate signaling. Dysfunction of CKIP-1 might constitutively activate NF-κB, leading to autoimmune diseases or malignant lymphomas, and the signaling events around CKIP-1 might be good therapeutic targets.

Supporting Information

Figure S1 Knockdown of CKIP-1 induces NF-κB activation. The JR-GFP cells were electroporated with 400 pmol of non-targeting siRNA, or specific siRNA against each gene by AMAXA Nucleofector System. Five days later, the expression of EGFP was assessed by FACS.
(TIF)

Acknowledgments

We thank Drs. T. Kitawaki and H. Fujita (University of Kyoto) for the manipulation of FACSAria cell sorter; Drs. T. Yoshida and T. Kobayashi (University of Kyoto) for the preparation of a human leukocyte-cDNA library; C. Sakamoto (University of Kyoto) for technical support.

Author Contributions

Conceived and designed the experiments: TS MK KT ATK. Performed the experiments: TS MK KN FI YT YA. Analyzed the data: KT MS KI KY KS NK. Contributed reagents/materials/analysis tools: KY YK. Wrote the paper: TS MK KS NK YK ATK.

References

1. Vallabhapurapu S, Karin M (2009) Regulation and function of NF-kappaB transcription factors in the immune system. Annu Rev Immunol 27: 693–733.
2. Kane LP, Lin J, Weiss A (2002) It's all Rel-ative: NF-kappaB and CD28 costimulation of T-cell activation. Trends Immunol 23: 413–420.
3. Dustin ML, Olszowy MW, Holdorf AD, Li J, Bromley S, et al. (1998) A novel adaptor protein orchestrates receptor patterning and cytoskeletal polarity in T-cell contacts. Cell 94: 667–677.
4. Dustin ML (2008) T-cell activation through immunological synapses and kinapses. Immunol Rev 221: 77–89.
5. Chuang HC, Lan JL, Chen DY, Yang CY, Chen YM, et al. (2011) The kinase GLK controls autoimmunity and NF-kappaB signaling by activating the kinase PKC-theta in T cells. Nat Immunol 12: 1113–1118.
6. Kong KF, Yokosuka T, Canonigo-Balancio AJ, Isakov N, Saito T, et al. (2011) A motif in the V3 domain of the kinase PKC-theta determines its localization in the immunological synapse and functions in T cells via association with CD28. Nat Immunol 12: 1105–1112.
7. Matsumoto R, Wang D, Blonska M, Li H, Kobayashi M, et al. (2005) Phosphorylation of CARMA1 plays a critical role in T Cell receptor-mediated NF-kappaB activation. Immunity 23: 575–585.
8. Sommer K, Guo B, Pomerantz JL, Bandaranayake AD, Moreno-Garcia ME, et al. (2005) Phosphorylation of the CARMA1 linker controls NF-kappaB activation. Immunity 23: 561–574.
9. Thome M, Charton JE, Pelzer C, Hailfinger S (2010) Antigen receptor signaling to NF-kappaB via CARMA1, BCL10, and MALT1. Cold Spring Harb Perspect Biol 2: a003004.
10. Blonska M, Lin X (2011) NF-kappaB signaling pathways regulated by CARMA family of scaffold proteins. Cell Res 21: 55–70.
11. Wang D, You Y, Case SM, McAllister-Lucas LM, Wang L, et al. (2002) A requirement for CARMA1 in TCR-induced NF-kappa B activation. Nat Immunol 3: 830–835.
12. Egawa T, Albrecht B, Favier B, Sunshine MJ, Mirchandani K, et al. (2003) Requirement for CARMA1 in antigen receptor-induced NF-kappa B activation and lymphocyte proliferation. Curr Biol 13: 1252–1258.
13. Hara H, Wada T, Bakal C, Kozieradzki I, Suzuki S, et al. (2003) The MAGUK family protein CARD11 is essential for lymphocyte activation. Immunity 18: 763–775.
14. Jun JE, Wilson LE, Vinuesa CG, Lesage S, Blery M, et al. (2003) Identifying the MAGUK protein Carma-1 as a central regulator of humoral immune responses and atopy by genome-wide mouse mutagenesis. Immunity 18: 751–762.
15. Newton K, Dixit VM (2003) Mice lacking the CARD of CARMA1 exhibit defective B lymphocyte development and impaired proliferation of their B and T lymphocytes. Curr Biol 13: 1247–1251.
16. Shaffer AL 3rd, Young RM, Staudt LM (2012) Pathogenesis of human B cell lymphomas. Annu Rev Immunol 30: 565–610.
17. Snow AL, Xiao W, Stinson JR, Lu W, Chaigne-Delalande B, et al. (2012) Congenital B cell lymphocytosis explained by novel germline CARD11 mutations. J Exp Med 209: 2247–2261.
18. Bosc DG, Graham KC, Saulnier RB, Zhang C, Prober D, et al. (2000) Identification and characterization of CKIP-1, a novel pleckstrin homology domain-containing protein that interacts with protein kinase CK2. J Biol Chem 275: 14295–14306.
19. Nie J, Liu L, He F, Fu X, Han W, et al. (2013) CKIP-1: a scaffold protein and potential therapeutic target integrating multiple signaling pathways and physiological functions. Ageing Res Rev 12: 276–281.
20. Safi A, Vandromme M, Caussanel S, Valdacci L, Baas D, et al. (2004) Role for the Pleckstrin Homology Domain-Containing Protein CKIP-1 in Phosphatidylinositol 3-Kinase-Regulated Muscle Differentiation. Mol Cell Biol 24: 1245–1255.
21. Canton DA, Olsten ME, Kim K, Doherty-Kirby A, Lajoie G, et al. (2005) The pleckstrin homology domain-containing protein CKIP-1 is involved in regulation of cell morphology and the actin cytoskeleton and interaction with actin capping protein. Mol Cell Biol 25: 3519–3534.
22. Zhang L, Xing G, Tie Y, Tang Y, Tian C, et al. (2005) Role for the pleckstrin homology domain-containing protein CKIP-1 in AP-1 regulation and apoptosis. EMBO J 24: 766–778.
23. Zhang L, Tie Y, Tian C, Xing G, Song Y, et al. (2006) CKIP-1 recruits nuclear ATM partially to the plasma membrane through interaction with ATM. Cell Signal 18: 1386–1395.
24. Tokuda E, Fujita N, Oh-hara T, Sato S, Kurata A, et al. (2007) Casein kinase 2-interacting protein-1, a novel Akt pleckstrin homology domain-interacting protein, down-regulates PI3K/Akt signaling and suppresses tumor growth in vivo. Cancer Res 67: 9666–9676.
25. Lu K, Yin X, Weng T, Xi S, Li L, et al. (2008) Targeting WW domains linker of HECT-type ubiquitin ligase Smurf1 for activation by CKIP-1. Nat Cell Biol 10: 994–1002.
26. Ling S, Sun Q, Li Y, Zhang L, Zhang P, et al. (2012) CKIP-1 Inhibits Cardiac Hypertrophy by Regulating Class II Histone Deacetylase Phosphorylation through Recruiting PP2A. Circulation.
27. Wang Y, Nie J, Zhang L, Lu K, Xing G, et al. (2012) CKIP-1 couples Smurf1 ubiquitin ligase with Rpt6 subunit of proteasome to promote substrate degradation. EMBO Rep 13: 1004–1011.
28. Wang D, Matsumoto R, You Y, Che T, Lin XY, et al. (2004) CD3/CD28 costimulation-induced NF-kappaB activation is mediated by recruitment of protein kinase C-theta, Bcl10, and IkappaB kinase beta to the immunological synapse through CARMA1. Mol Cell Biol 24: 164–171.
29. Cvijic ME, Xiao G, Sun SC (2003) Study of T-cell signaling by somatic cell mutagenesis and complementation cloning. Journal of Immunological Methods 278: 293–304.
30. Kawano Y, Yoshida T, Hieda K, Aoki J, Miyoshi H, et al. (2004) A lentiviral cDNA library employing lambda recombination used to clone an inhibitor of

human immunodeficiency virus type 1-induced cell death. J Virol 78: 11352–11359.
31. Yoshida T, Kawano Y, Sato K, Ando Y, Aoki J, et al. (2008) A CD63 Mutant Inhibits T-cell Tropic Human Immunodeficiency Virus Type 1 Entry by Disrupting CXCR4 Trafficking to the Plasma Membrane. Traffic 9: 540–558.
32. Baier-Bitterlich G, Uberall F, Bauer B, Fresser F, Wachter H, et al. (1996) Protein kinase C-theta isoenzyme selective stimulation of the transcription factor complex AP-1 in T lymphocytes. Mol Cell Biol 16: 1842–1850.
33. Wertz IE, O'Rourke KM, Zhou H, Eby M, Aravind L, et al. (2004) De-ubiquitination and ubiquitin ligase domains of A20 downregulate NF-kappaB signalling. Nature 430: 694–699.
34. Gaide O, Favier B, Legler DF, Bonnet D, Brissoni B, et al. (2002) CARMA1 is a critical lipid raft-associated regulator of TCR-induced NF-kappa B activation. Nat Immunol 3: 836–843.
35. Bromley SK, Burack WR, Johnson KG, Somersalo K, Sims TN, et al. (2001) The immunological synapse. Annu Rev Immunol 19: 375–396.
36. Blonska M, Lin X (2009) CARMA1-mediated NF-kappaB and JNK activation in lymphocytes. Immunol Rev 228: 199–211.
37. Lenz G, Davis RE, Ngo VN, Lam L, George TC, et al. (2008) Oncogenic CARD11 mutations in human diffuse large B cell lymphoma. Science 319: 1676–1679.
38. Ngo VN, Davis RE, Lamy L, Yu X, Zhao H, et al. (2006) A loss-of-function RNA interference screen for molecular targets in cancer. Nature 441: 106–110.
39. Lim KH, Yang Y, Staudt LM (2012) Pathogenetic importance and therapeutic implications of NF-kappaB in lymphoid malignancies. Immunol Rev 246: 359–378.
40. Brdicka T, Pavlistova D, Leo A, Bruyns E, Korinek V, et al. (2000) Phosphoprotein associated with glycosphingolipid-enriched microdomains (PAG), a novel ubiquitously expressed transmembrane adaptor protein, binds the protein tyrosine kinase csk and is involved in regulation of T cell activation. J Exp Med 191: 1591–1604.
41. Davidson D, Bakinowski M, Thomas ML, Horejsi V, Veillette A (2003) Phosphorylation-dependent regulation of T-cell activation by PAG/Cbp, a lipid raft-associated transmembrane adaptor. Mol Cell Biol 23: 2017–2028.
42. Hayden MS, Ghosh S (2008) Shared principles in NF-kappaB signaling. Cell 132: 344–362.
43. Dobenecker MW, Schmedt C, Okada M, Tarakhovsky A (2005) The ubiquitously expressed Csk adaptor protein Cbp is dispensable for embryogenesis and T-cell development and function. Mol Cell Biol 25: 10533–10542.
44. Xu S, Huo J, Tan JE, Lam KP (2005) Cbp deficiency alters Csk localization in lipid rafts but does not affect T-cell development. Mol Cell Biol 25: 8486–8495.
45. Oneyama C, Hikita T, Enya K, Dobenecker MW, Saito K, et al. (2008) The lipid raft-anchored adaptor protein Cbp controls the oncogenic potential of c-Src. Mol Cell 30: 426–436.
46. Krishna S, Xie D, Gorentla B, Shin J, Gao J, et al. (2012) Chronic activation of the kinase IKKbeta impairs T cell function and survival. J Immunol 189: 1209–1219.
47. Lamason RL, Kupfer A, Pomerantz JL (2010) The dynamic distribution of CARD11 at the immunological synapse is regulated by the inhibitory kinesin GAKIN. Mol Cell 40: 798–809.
48. Bidere N, Ngo VN, Lee J, Collins C, Zheng L, et al. (2009) Casein kinase 1alpha governs antigen-receptor-induced NF-kappaB activation and human lymphoma cell survival. Nature 458: 92–96.

VIP Real-Time NMR Spectroscopy Very Important Paper

DOI: 10.1002/anie.201309940

Quantitative Analysis of Location- and Sequence-Dependent Deamination by APOBEC3G Using Real-Time NMR Spectroscopy**

*Ayako Furukawa, Kenji Sugase, Ryo Morishita, Takashi Nagata, Tsutomu Kodaki, Akifumi Takaori-Kondo, Akihide Ryo, and Masato Katahira**

Abstract: *The human antiretroviral factor APOBEC3G (A3G) deaminates the newly synthesized minus strand of the human immunodeficiency virus 1 (HIV-1), which results in the abolition of the infectivity of virus-infectivity-factor (Vif)-deficient HIV-1 strains.[1–6] A unique property of A3G is that it deaminates a CCC hot spot that is located close to the 5′ end more effectively than one that is less close to the 5′ end. However, the mechanism of this process is elusive as it includes nonspecific binding of A3G to DNA and sliding of A3G along the DNA strand. Therefore, this process cannot be analyzed by existing methods using the Michaelis–Menten theory. A new real-time NMR method has been developed to examine the nonspecific binding and the sliding processes explicitly, and it was applied to the analysis of the deamination by A3G. As a result, the location-dependent deamination can be explained by a difference in the catalytic rates that depend on the direction of the approach of A3G to the target cytidine. Real-time NMR experiments also showed that A3G deaminates CCCC tandem hotspots with little redundancy, which suggests that A3G efficiently mutates many CCC hotspots that are scattered throughout the HIV-1 genome.*

The enzyme APOBEC3G (A3G) possesses two consensus zinc-finger-type cytidine deaminase motifs (CD1 and CD2),[2] but only CD2 is catalytically active.[7,8] A3G preferably deaminates the third cytidine of a CCC sequence in single-stranded DNA (ssDNA).[9,10] It was reported that A3G nonspecifically binds to ssDNA and slides along ssDNA over 30 nm (69 nucleotides) without directional preference.[11,12] Interestingly, A3G deaminates CCC hot spots in a location-dependent fashion.[10] A 5′ to 3′ gradient of mutations in HIV RNA, which is transcribed from the minus strand DNA, was observed in vivo.[9,13] This would arise from the 3′ to 5′ deamination gradient of minus strand DNA by A3G. Deamination by A3G has been analyzed by various methods, including gel shift assays,[10,14,15] single-molecule fluorescence resonance energy transfer (FRET) spectroscopy,[11] and atomic force microscopy.[12,16] We previously demonstrated that real-time NMR spectroscopy can be utilized to monitor the deamination reaction and revealed that A3G CD2 deaminates the third cytidine of CC<u>C</u> much faster than the second one (C<u>C</u>C).[17] An advantage of real-time NMR spectroscopy over other methods is that it can directly detect a site-specific deamination reaction. Moreover, this method is sensitive to weak interactions because highly concentrated ssDNA (mM order) can be used for the NMR experiment. The real-time NMR method that we used for the analysis of the deamination process has become increasingly popular and has been used by other groups.[18,19]

Our real-time NMR method monitors the intensity change of the H5–H6 total correlation spectroscopy (TOCSY) peak of the third cytidine of CC<u>C</u> in real time. Using this method, we previously analyzed the deamination of a hot spot that solely exists in ssDNA. To gain insight into the mechanism that underlies the location-dependent deamination by A3G, we further developed this NMR method. First, to determine whether real-time NMR spectroscopy provides sufficiently high spectral and time resolution to distinguish the multiple deamination reactions that occur on ssDNA, we monitored the deamination reactions of ssDNA comprising two CCC hot spots (S_{2CCC} in Table 1; see also the Supporting Information). Obviously, the two hot spots were deaminated at different rates by full-length A3G (Figure 1 a). Surprisingly, CD2 alone also deaminated the two hot spots in a location-dependent manner, exhibiting higher activity than full-length A3G (Figure 1 b). The higher activity of A3G CD2 was previously observed by Chen and co-workers.[14] F-tests showed that the difference between the deamination rates for

[*] Dr. A. Furukawa, Prof. T. Nagata, Prof. T. Kodaki, Prof. M. Katahira
Institute of Advanced Energy, Graduate School of Energy Science
Kyoto University
Gokasho, Uji, Kyoto 611-0011 (Japan)
E-mail: katahira@iae.kyoto-u.ac.jp
Dr. K. Sugase
Bioorganic Research Institute, Suntory Foundation for Life Sciences
1-1-1 Wakayamadai, Shimamoto, Mishima, Osaka 618-8503 (Japan)
Dr. R. Morishita
CellFree Sciences Co., Ltd., Ehime University Venture
Matsuyama, Ehime 790-8577 (Japan)
Prof. A. Takaori-Kondo
Department of Hematology and Oncology
Graduate School of Medicine, Kyoto University
54 Shogoin-Kawaracho, Sakyo-ku, Kyoto 606-8507 (Japan)
Dr. R. Morishita, Prof. A. Ryo
Department of Microbiology
Yokohama City University School of Medicine
3-9 Fukuura, Kanazawa-ku, Yokohama 236-0004 (Japan)

[**] We thank the Ministry of Education, Science, Sports and Culture of Japan for Grants-in Aid for Scientific Research (24121714, 25115507, and 25291013 to M.K.; 23570146 and 24113710 to T.N.), Japan Science and Technology (CREST; M.K.), the Sumitomo–Denko and Iwatani Foundations (M.K.), and the Japan Society for the Promotion of Science (A.F.). For funding for open access charges, we are grateful to the Ministry of Education, Science, Sports and Culture of Japan (24121714).

Supporting information for this article is available on the WWW under http://dx.doi.org/10.1002/anie.201309940.

Table 1: Oligonucleotides used in this study.

Name	Sequence
S_{2CCC}	ATTCCCAATTTTTTTTATACCCATTT
$S_{CCCssCCC}$	ATTCCCAATTTTTTTTTTTTTTTTTTTATACCCAT$_{23}$
$S_{CCCdsCCC}$	ATTCCCAATTCGCGAACGCGCAAGCGCATACCCAT$_{23}$ GCGCTTGCGCGTTCGCG
$S_{5'CCC}$	TTACCCAT$_{42}$
S_{mCCC}	T$_{21}$ACCCAT$_{22}$
$S_{3'CCC}$	T$_{41}$ACCCATTT
S_{CCCC}	ATTCCCCATT
S_{CCCU}	ATTCCCUATT
S_{CCUC}	ATTCCUCATT
S_{CCCA}	ATTCCCAATT
S_{CCUA}	ATTCCUAATT
S_{CCUU}	ATTCCUUATT

The cytidines that are to be deaminated are underlined.

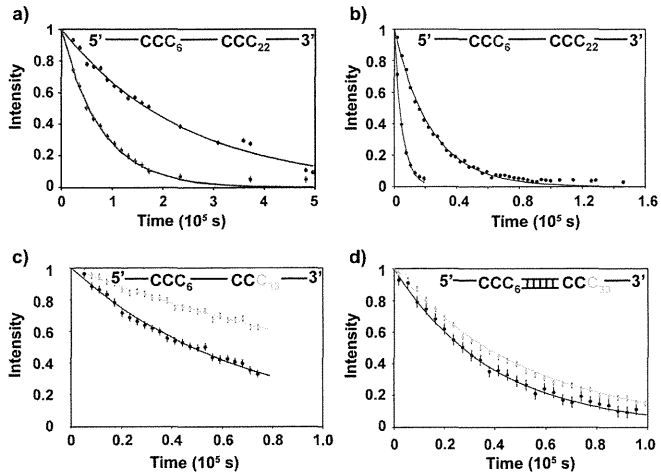

Figure 1. Real-time monitoring of deamination reactions at two CCC hot spots in ssDNA. a, b) Deamination reactions with full-length A3G (a) and CD2 (b) were monitored for C6 (●) and C22 (●) in S_{2CCC}. The deamination rates for full-length A3G are $1.3\times10^{-5}\pm4.0\times10^{-7}$ s^{-1} for C6 and $4.1\times10^{-6}\pm7.4\times10^{-8}$ s^{-1} for C22, and those for CD2 are $2.0\times10^{-4}\pm7.5\times10^{-6}$ s^{-1} for C6 and $4.2\times10^{-5}\pm5.0\times10^{-7}$ s^{-1} for C22. c, d) Deamination reactions of CD2 were monitored for C6 (●) and C33 (●) in $S_{CCCssCCC}$ (c) and $S_{CCCdsCCC}$ (d).

the two hot spots is statistically significant for both full-length A3G and CD2. The same result was obtained with ssDNA in which two units of S_{2CCC}, ATTCCCAAT and ATACCCATT, had swapped positions. These results confirmed that CD2 alone causes the location-dependent deamination. Although catalytically inactive CD1 also supposedly contributes to the location-dependent deamination process, we assumed that the intrinsic characteristics of CD2 are important for the location-dependent deamination by full-length A3G. We focused on CD2 in the following experiments. Subsequently, we investigated whether our real-time NMR method can be used to examine the sliding of A3G along ssDNA. As A3G binds to ssDNA, but not to dsDNA,[10] intervening dsDNA should block the sliding of A3G. As shown in Figure 1c and d, the deamination rates of two hot spots in a substrate with short dsDNA between them were almost the same, whereas the rates were location-dependent without dsDNA ($S_{CCCdsCCC}$ and $S_{CCCssCCC}$ in Table 1). This finding clearly indicates that real-time NMR spectroscopy can sense the sliding of A3G CD2 along ssDNA.

We have thus confirmed that real-time NMR spectroscopy is sufficiently sensitive to location-dependent deamination reactions and sliding processes of A3G CD2. Based on these results, we designed experiments and constructed a kinetic model to quantitatively analyze the deamination reaction. As A3G binds to ssDNA nonspecifically, the binding rate should depend on the length of the ssDNA and the concentrations of A3G and ssDNA. On the other hand, the duration of the sliding to reach a hot spot should depend on the length of the ssDNA and the position of a hot spot. Therefore, the kinetics of the deamination reaction can be determined by real-time NMR studies with different concentrations of ssDNA and A3G CD2, and with ssDNAs of different lengths and with different positions of hot spots. According to this idea, we developed a kinetic model for the analysis of real-time NMR data (see the Supporting Information). The deamination reaction that is monitored by NMR spectroscopy as a change of intensity, $I(t)$, is expressed as:

$$I(t) = I_0\exp(-k_{deami}t) \quad (1)$$

I_0 is the initial intensity, which is proportional to the concentration of ssDNA, and k_{deami} represents the apparent deamination rate, which is calculated as detailed below:

$$k_{deami} = \frac{[^NS][^NE]}{S_0K_d}\left\{k_{cat(3'\rightarrow5')}(1-\alpha^n) + k_{cat(5'\rightarrow3')}\left(1-\alpha^{N-n+1}\right)\right\} \quad (2)$$

$$[^NS] = \frac{1}{2}\left(-{}^N\beta + S_0 - E_0 + \sqrt{({}^N\beta - S_0 + E_0)^2 + 4E_0{}^N\beta}\right) \quad (3)$$

$$[^NE] = \frac{1}{2}\left(-{}^N\beta - S_0 + E_0 + \sqrt{({}^N\beta + S_0 - E_0)^2 + 4E_0{}^N\beta}\right) \quad (4)$$

$$\alpha = k_s/(k_s + k_{off}), \quad {}^N\beta = \frac{K_d}{2\{N+1-(1-\alpha^{N+1})/(1-\alpha)\}} \quad (5)$$

N and n represent the total number of nucleotides in ssDNA and the position of the reacting cytidine from the 3' end, respectively. According to this kinetic model, A3G CD2 binds to any nucleotide of ssDNA with an association rate constant k_{on} and dissociates from ssDNA with a dissociation rate constant k_{off}. A3G CD2 slides along ssDNA in both directions at a sliding rate k_s (Figure 2a). As the ssDNAs used are relatively short (49–57 nucleotides), we assumed that the sliding of A3G CD2 does not change direction during a single sliding event. The structure of the A3G–ssDNA complex has not been determined yet; therefore, it is still unknown how A3G recognizes a hot spot. On the other hand, the structure of free A3G CD2 has already been determined, and a protruding bump that hangs over one side of the catalytic pocket, which includes the catalytic residue Glu259 and the zinc ion, was revealed (Supporting Information, Figure S1a).[14,17,20] We assumed that this bump interferes with the accommodation of the target cytidine into the catalytic pocket; this process depends on the direction of the approach of A3G CD2 (Figure S1b,c). Then, we incorporated two cata-

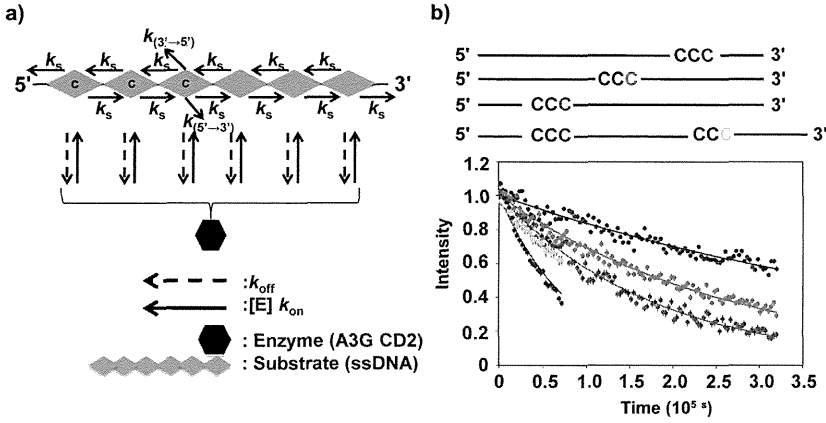

Figure 2. Quantitative analysis of the location-dependent deamination reaction using real-time NMR spectroscopy. a) Kinetic model of the deamination reaction by A3G. b) Real-time NMR data for C6 of $S_{5'CCC}$ (●), C26 of S_{mCCC} (●), C45 of $S_{3'CCC}$ (●), and both C6 (●) and C33 (●) of $S_{CCCssCCC}$ were fitted to Eq. (1).

lytic rates, $k_{cat(3'\rightarrow5')}$ and $k_{cat(5'\rightarrow3')}$, into the model, which are the catalytic rates for the cases where A3G CD2 approaches the target cytidine from downstream and upstream, respectively. As A3G slides along ssDNA without directional preference,[12] the location-dependent deamination is difficult to explain without the two different k_{cat} values. These k_{cat} values represent the rates of the entry of ssDNA into the catalytic pocket and of its deamination. A global fit of multiple real-time NMR data collected under different conditions (see above) provided the parameters α, K_d ($=k_{off}/k_{on}$), $k_{cat(3'\rightarrow5')}$, and $k_{cat(5'\rightarrow3')}$. However, it is difficult to separate α into k_s and k_{off} because neither the sliding nor the dissociation process can be perturbed experimentally without affecting the other process. The NMR data were fitted to Eq. (1) using the program GLOVE.[21]

For this analysis, we obtained real-time NMR data for $S_{5'CCC}$, S_{mCCC}, and $S_{3'CCC}$ (Table 1) aside from the data for the aforementioned two hot spots of $S_{CCCssCCC}$. These data are in good agreement with Eq. (1), yielding values for $k_{cat(3'\rightarrow5')}$ and $k_{cat(5'\rightarrow3')}$ of 68 s^{-1} and 14 s^{-1}, respectively (Figure 2b). The closer a CCC hot spot is located to the 5′ end, the more chance it has of being detected by A3G approaching from downstream rather than from upstream; therefore, a CCC hot spot that is located close to the 5′ end is deaminated more rapidly than one that is less close to the 5′ end.

For further applications of our real-time NMR method, we analyzed the deamination of CCCC, in which two CCC sequences overlap (S_{CCCC} in Table 1). The clusters of three to six consecutive cytidines are scattered throughout the HIV genome, and CCCC is the second most abundant cluster after CCC. Unfortunately, the NMR peaks that need to be monitored during the deamination reactions overlapped, for example, the TOCSY peaks of the fourth cytidines of CCCC and CCUC. Therefore, the time courses of each deamination reaction could not be monitored separately (Figure 3a and b). However, the results of the deamination reactions were characterized using the NMR spectrum of the same ssDNA whose deamination reactions had reached completion. As a result, the third and fourth cytidines of CCCC were found to be deaminated by A3G CD2 with equal efficiency because the intensities of peaks 2 (CCUC) and 3 (CCCU + CCUU) were nearly identical. This finding is different from that of a previous study with a gel shift assay; in the earlier case, the third cytidine was deaminated more efficiently than the fourth cytidine.[15] This discrepancy could be due to the difference in the duration of the monitoring between our NMR method (6 h) and the gel shift assay (3 min). Real-time NMR spectroscopy can monitor multiple reactions directly and simultaneously using a single sample, whereas the gel shift assay cannot. Therefore, our results should provide more accurate information.

The deamination of CCCU into CCUU is redundant and may be unnecessary for abolition of the HIV infectivity. However, the above experiment could not provide information on the deamination efficiency for CCCU because the NMR peaks of CCUU and CCUC overlapped. Thus, we monitored the deamination reactions for CCCA (non-deaminated site) and CCCU (monodeaminated site) to determine whether or not A3G has a preference for either of the two sequences, S_{CCCA} and S_{CCCU} (Table 1). In this case, the deamination reactions were monitored by one-dimensional ^{1}H NMR spectroscopy to increase spectral resolution (Figure 3c and d). The results revealed that A3G preferentially deaminates a non-deaminated site rather than a monodeami-

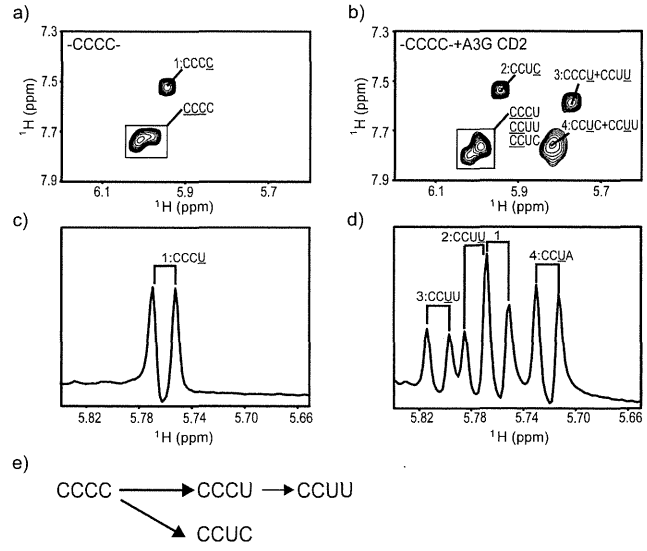

Figure 3. Deamination reactions of CCCC by A3G CD2. a, b) TOCSY spectrum of S_{CCCC} (a) and TOCSY spectrum recorded six hours after the addition of A3G CD2 (b). The peaks are labeled with the sequences of the corresponding substrates or deaminated products in which the assigned residues are underlined (see the Supporting Information). c, d) ^{1}H NMR spectrum of an equimolar mixture of S_{CCCA} and S_{CCCU} (c), and ^{1}H NMR spectrum recorded 40 minutes after the addition of A3G CD2 (d). Peaks 1 to 4 were assigned by recording the NMR spectra of S_{CCUU} and S_{CCUA}. e) Two possible deamination reaction pathways for CCCC.

